HHS Public Access

Author manuscript

Acta Biomater. Author manuscript; available in PMC 2020 September 01.

Published in final edited form as:

Acta Biomater. 2019 September 01; 95: 3–31. doi:10.1016/j.actbio.2018.11.040.

Cell Armor for Protection Against Environmental Stress: Advances, Challenges and Applications in Micro- and Nanoencapsulation of Mammalian Cells

Onur Hasturk[a], **David L. Kaplan**[a,*]

[a]Department of Biomedical Engineering, Tufts University, Medford, MA 02155, USA

Abstract

Unlike unicellular organisms and plant cells surrounded with a cell wall, naked plasma membranes of mammalian cells make them more susceptible to environmental stresses encountered during *in vitro* biofabrication and *in vivo* cell therapy applications. Recent advances in micro- and nanoencapsulation of single mammalian cells provide an effective strategy to isolate cells from their surroundings and protect them against harsh environmental conditions. Microemulsification and droplet-based microfluidics have enabled researchers to encapsulate single cells within a variety of microscale hydrogel materials with a range of biochemical and mechanical properties and functionalities including enhanced cell-matrix interactions or on-demand degradation. In addition to microcapsules, nanocoatings of various organic and inorganic substances on mammalian cells have allowed for the formation of protective shells. A wide range of synthetic and natural polymers, minerals and supramolecular metal-organic complexes have been deposited as nanolayers on the cells via electrostatic interactions, receptor-ligand binding, non-specific interactions, and *in situ* polymerization/crosslinking. Here, current strategies in encapsulation of single mammalian cells along with challenges and advances are reviewed. Protection of encapsulated stem cells, fibroblasts, red and white blood cells and cancer cells against harsh *in vitro* and *in vivo* conditions including anoikis, UV radiation, physical forces, proteolytic enzymes and immune clearance are discussed.

Graphical Abstract

*Corresponding author. E-mail address: david.kaplan@tufts.edu (David L. Kaplan).

Conflict of Interest

The authors declare that they have no conflicts of interest.

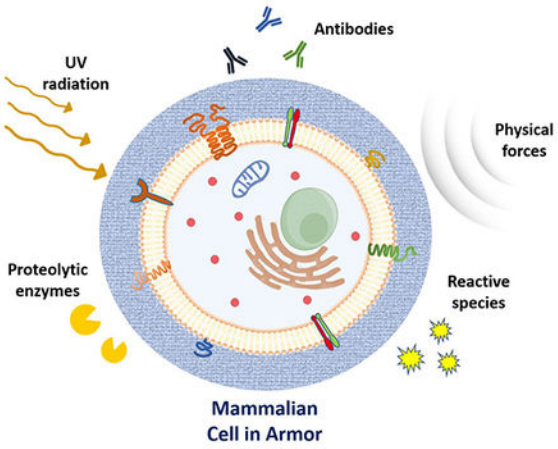

Keywords

single cell encapsulation; mammalian cells; microgels; nanocoatings; protective shells

1. Introduction

Use of stem or tissue specific cells in systemic transplantation or in *ex vivo* engineered tissue-like constructs in cell therapy and tissue engineering applications holds promise to fight diseases [1–5] and to maintain, recover or replace the functions of failing organs damaged by age, injury or disease [6, 7]. Both cell therapy and tissue engineering applications require *ex vivo* handling and manipulation of cells. Mammalian cells, particularly adult stem cells that have the ability of self-renewal and differentiation into multiple lineages [8] are, however, challenging to handle *ex vivo* due to their susceptibility to environmental conditions. Unlike prokaryotes, unicellular eukaryotes or fungi, animal cells do not have a strong cell wall or exoskeletal shell to provide structural support. Despite the internal cytoskeletal network, fluidic plasma membrane enclosing mammalian cells is fragile and makes the cells susceptible to harsh environmental conditions during manipulation, handling or storage. Physical forces are one of the most inevitable environmental stress that cells face during both *in vitro* and *in vivo* applications. For example, lymphocytes and stem cells are subjected to shear stress in the needle during their intravenous injection or in the venous system under fluid flow [1–3]. Shear and extensional forces are also generated during *in vitro* applications, such as in microfluidic cell analysis, bioreactor cultures and even centrifugation for the collection or separation of cells. These mechanical stresses may reduce the viability of the cells due to the damaged plasma membrane and the subsequent leakage of cytosolic components [9–11].

An important *in vitro* method during which mammalian cells are exposed to a variety of physical and chemical stresses is the three-dimensional (3D) bioprinting. Advances in biofabrication by 3D bioprinting has enabled researchers to generate complex tissue and organ systems. During the last decade, a variety of cells, biomolecules and bioink materials have been reported for the layer-by-layer printing of cell-laden hydrogels with a wide range of shapes, structures and mechanical properties for variable target tissues. Despite its control

over structure, high spatial resolution, speed and cost effectiveness, challenges in maintaining the function and viability of the printed cells significantly limits the applications of 3D bioprinting. Cells should be able to resist the crosslinking conditions (Fig. 1), such as the fluctuations in temperature, changes in solution pH, and the presence of reactive species for chemically-crosslinked hydrogels or for exposure to UV light for photo-crosslinked hydrogels [12–16]. The main factor that compromises the function and viability of encapsulated cells, however, is the shear stress inflicted during the extrusion of high viscosity bioinks through a thin nozzle [17]. For the non-Newtonian laminar flow of a cell-laden pre-hydrogel solution through a syringe and nozzle system, shear stress is a function of shear rate as follows [18]

$$\tau = m\gamma^n \quad (1)$$

where τ is the shear stress, γ is the shear rate, and n and m are the experimentally determined power-law index and power-law consistency coefficients of the hydrogel material, respectively. Assuming a uniform flow rate in the syringe and no change in the volume of hydrogel before and after printing, the speed of the extruded hydrogel (V_2) and the shear rate in the nozzle (γ) can be expressed as follows

$$V_2 = V_1\left(\frac{R_1}{R_2}\right)^2 \quad (2)$$

$$\gamma^n = \left[\frac{V_2 {R_2}^2}{\left(\frac{n}{3n+1}\right)\left(R_2^{\frac{3n+1}{n}}\right)}\right]^n \cdot r \quad (3)$$

where V_1 is the speed of the piston, R_1 is the radius of the syringe chamber, R_2 is the inner radius of the nozzle, and r is the radial distance from the axis of nozzle. The shear rate and shear stress increase with an increase in the radial distance from the axis of the nozzle and reaches its maximum value at the nozzle wall (Fig. 1b). Depending on the printing parameters, the extremes of shear forces applied near the walls of the nozzle may disrupt the integrity of the plasma membrane and negatively impact the cells. Shear stress created in the extrusion nozzle during 3D bioprinting has been reported to form nanoscale pores on the plasma membrane of the cells [19] and dramatically reduce the viability of printed cells [12, 17, 20]. Even though extrusion-induced shear stress can be reduced by printing lower viscosity bioinks with larger nozzles at lower pressures, the drawback would be the loss of resolution and printing speed. Moreover, even moderate levels of shear stress can modulate proliferation and differentiation of stem cells [17, 21], which may cause deviations from the intended application. Therefore, it has been of increasing interest to protect the cells from physical and chemical stresses during the bioprinting process.

One approach to protect mammalian cells from harsh environmental conditions has been the isolation of cells from their surroundings through encapsulation within a biocompatible protective shell. Earlier research for this purpose started with micro- and nanoencapsulation of multiple cells. Microfluidics-based microencapsulation strategies using a variety of hydrogel systems were proposed for cell-based drug delivery [22] and transplantation purposes [23, 24], while nanocoatings of soft polymers and hydrogels were reported for the nanoencapsulation of pancreatic cell clusters [25–29]. This was followed by the field of single cell encapsulation, which has been growing rapidly during the last decade. First, microfluidic strategies have been adapted for immobilization of single mammalian cells in microgels by optimization of cell concentrations and droplet formation rates [23, 24]. Early research in nanoencapsulation of single cells, on the other hand, started with sacrificial fixed cells for the formation of hollow microcapsules and then advanced to the encapsulation of living bacteria and yeasts [27, 30]. Various strategies for nanoencapsulation of bacteria and yeasts were proposed for the formation of “artificial spores” and “cell-in-shell” structures [31–34] for several biotechnology applications including whole-cell biocatalysis or probiotic delivery [34, 35]. Later, these strategies were then adapted for nanocoating of mesenchymal stem cells, immune cells and red blood cells with thin layers of polyelectrolytes, mineral shells and supramolecular metal-organic complexes [32, 36]. In this review paper, recent strategies and challenges of the micro- and nanoencapsulation of individual mammalian cells are discussed. Protection of the encapsulated cells from environmental conditions such as cytotoxic compounds, mechanical stress and UV radiation is also emphasized to highlight the potential applications of the approach. Advances will be focused only on the encapsulation of single mammalian cells and any approach including multiple cells or unicellular organisms will be excluded.

2. Approaches for Encapsulation of Individual Mammalian Cells

2.1. Microencapsulation

Microencapsulation of cells (Table 1) has been an attractive strategy to overcome the challenges of bioprocesses by providing protection from environmental conditions such as hydrodynamic shear and immune attack while allowing for the efficient transfer of nutrients, gases and cellular wastes through the microcapsule matrix. Microencapsulated cells can be stored and manipulated in a controlled manner ex vivo. Encapsulation of single cells into biomatrices such as hydrogels enables researchers to tune the physico- and biochemical properties of the cell microenvironment to mimic natural environments *in vivo*. Downsizing the matrix to the micrometer scale offers unique advantages of improved diffusion rates of solutes through efficient material-to-cell volume ratios in a 3D culture environment [24, 30, 37, 38]. The use of single cell-laden microbeads may also help reduce the amounts of biochemical factors incorporated into the systems without changing the physiological concentrations around the cells, thus, lowering the risk of potential adverse effects and therapy costs without compromising the overall performance of the cells [39].

Microemulsification of aqueous solutions in an oil phase has been reported as a method for single cell microencapsulation. In an early study, Karoubi et al. reported encapsulation of single human MSCs (hMSCs) in agarose capsules supplemented with cell adhesive matrix

proteins fibronectin and fibrinogen (f/f) [1]. A suspension of hMSCs with agarose-(f/f) in phosphate buffered saline (PBS) was added dropwise into dimethylpolysiloxane and emulsified by vortexing. The gelation of agarose was triggered by cooling down the mixture in an ice bath, resulting in hMSCs encapsulated in agarose cocoons of 20 – 50 μm diameter (Fig. 2A). The concentration of the cells in suspension was adjusted so that most of the cell-laden agarose capsules contained single cells. This, however, resulted in 85% of the agarose microgels being empty. The survival rate of the encapsulated cells was over 90%, indicating that the encapsulation process was not detrimental to the cells. The same strategy was employed also for the microencapsulation of human cardiac stem cells (hCSCs) [2]. This time, however, the proportion of the microgels with multiple cells was much higher (around 30% of all cell-laden microgels) compared to the previous study (Fig. 2B). The encapsulation process preserved both cell viability and secretion of cardio-protective and pro-angiogenic cytokines. Under hypoxic (1% O_2) conditions, secretion of angiogenin, stromal cell-derived factor-1 (SDF-1), vascular endothelial growth factor (VEGF) and interleukin-6 (IL-6) was higher compared to native cells in suspension.

An interesting strategy was reported by Lahann and co-workers, who utilized a modified electrospraying method for the encapsulation of single NIH3T3 mouse fibroblasts in the core of biodegradable poly(lactide-co-glycolide) (PLGA) shells [40]. Briefly, cell suspensions in bovine serum albumin (BSA) solutions were emulsified in PLGA dissolved in a mixture of chloroform and dimethyl fumarate (DMF) and the mixture was sprayed through a needle using coaxial electrohydrodynamic jetting (EHD) at high electrical voltage (Fig. 2C-i). Cells entrapped within the core of PLGA shells were obtained upon the rapid evaporation of both water and the organic solvents from the droplets. The influence of BSA concentration, core flow rate, polymer concentration, chloroform:dimethylformamide (DMF) ratio and shell flow rate on the encapsulation efficiency, core size and particle yield were investigated to optimize the formation of particles. The shell flow rate and solvent ratio determined the particle yield, while the core flow rate and BSA concentration affected the microencapsulation efficiency. The target core diameter was designed as 8–10 μm to encapsulate single mammalian cells (Fig. 2C-ii), determined by the shell solvent ratio, core flow rate and shell flow rate. After optimization of these experimental factors, cells were successfully encapsulated in PLGA core-shell particles (Fig. 2C-iii), and ~75% of the encapsulated cells survived the applied electric potential during EHD jetting.

2.1.1. Encapsulation by Droplet-based Microfluidics—The advances in microfabrication and poly(dimethylsiloxane) (PDMS)-based soft lithography methods accelerated the fabrication of microfluidic devices, allowing precise control of small volumes of fluids within microscale channels [41, 42]. The interest in production of aqueous droplets using microfluidics has been growing because it enables the rapid production of monodisperse microdroplets with diameters of ten to hundreds of μm. Droplet-based microfluidics are based on the fabrication of aqueous emulsions in an immiscible carrier oil such as mineral, vegetable, or fluorinated oils. Femto-, pico- or even nanoliter aqueous compartments produced by microfluidics have been utilized as microreactors or cargo for particles, biomolecules such as metabolites, proteins and DNA [41]. In the last few years, droplet microfluidics has been employed as a rapid, accurate and cost-effective method for

single cell encapsulation. Encapsulation into picolitre volumes enable qualitative and quantitative studies of single cells in a large population by isolating them from other cells or their environments. The small volume of the droplet entraps the components or secretion products of individual cells, and the minimized diffusion through the oil-water interface keeps the concentration relatively constant [43–45]. This system allows for dynamic living cell assays, single cells immunoanalysis [46], high throughput screening (HTS) applications involving drug discovery, toxicity testing and rare cell analysis [41], and characterization of individual cells at the genomic or transcriptomic level with shorter reaction times, higher sensitivity and throughput without cross contamination [42, 45]. The geometries of the microfluidic devices that have been commonly used for droplet production include co-flowing, T-junction and flow-focusing constructs (Fig. 3A). The operation principle of all three is based on the interface created between two immiscible fluids that co-flow through microfluidic channels. Droplets are formed when one of the fluid streams self-segregates upon being surrounded by the second fluid. Among the three geometries, the most widely employed structure for the microencapsulation of single cells has been the flow-focusing design, in which a continuous oil stream surrounds the dispersing aqueous stream containing the cells; the oil shear periodically breaks off the water droplet from the flowing aqueous stream [24, 44, 47]. The size and formation rate of the droplets depends on the dimensions of the microchannels and the flow rates, viscosities and polarities of the aqueous and oil phases [23, 24, 30, 41, 44].

An early example of droplet-based microfluidics for the encapsulation of single cells included the coating of aqueous droplets with lipid bilayers for the encapsulation of live HeLa and MCF-7 breast cancer cells [48]. Aqueous droplets with single cells were created in the lipid phase that consisted of oleic acid as the solvent and the phospholipids 1,2-Dioleoyl-sn-Glycero-3Phosphocholine (DOPC), 1,2-Dimyristoyl-sn-Glycero-3-Phosphocholine (DMPC) and 1,2-Dipalmitoyl-sn-Glycero-3-Phosphocholine (DPPC) (Fig. 3B-i). Upon interaction of the polar head groups of the phospholipids with the aqueous phase, a phospholipid monolayer was formed around the droplets. The emulsion solution was then injected into the aqueous mixture of water and ethanol, which forced the phospholipids dissociated from the liquid phase to rearrange around the droplets and assemble into lipid bilayers (Fig. 3B-ii). The increase in the flow rate of the lipid phase during droplet formation decreased the size of the droplets and increase their stability. The flow rates of the fluids within the microfluidic device and the concentration of ethanol used in dissolution bath influenced vesicle yield and encapsulation efficiency. The vesicles produced using this approach were stable in aqueous media over 26 days. The average size of the cell encapsulating vesicles was adjusted to 60 μm with 20% variation. Both HeLa and MCF-7 (Fig. 3B-iii) cells encapsulated in lipid vesicles were viable 2 h after the encapsulation process, indicating negligible cytotoxicity of the chemicals and the methods used.

In addition to aqueous droplets, droplet microfluidics has also been utilized for the encapsulation of single cells within microspheres of polymer hydrogels with tunable compositions and mechanical properties. Typically, cells are suspended in a biocompatible and rapidly gelating pre-hydrogel solution. This mixture is then used as the disperse phase of a droplet-based microfluidic setup, and the precursor droplets are exposed to a curing method to obtain hydrogel microcapsules [41]. The method used for gelation varies with the

material used. Chemically reactive materials such as poly(ethylene glycol) (PEG) are crosslinked in the presence chemoinitiators or photoinitators with light (e.g., UV) exposure. Physical gelation occurs by thermosetting or ionic crosslinking. The gelation of thermoresponsive materials such as agarose and gelatin (GL) is triggered by cooling [23, 30].

Hydrogel systems formed by chemical crosslinking of two polymers upon mixing without using any initiators have been utilized for the microencapsulation of single cells. In this approach, two polymer solutions were injected separately through parallel inlets and the streams were mixed just before the flow-focusing junction, resulting in rapid gelation of the droplets shortly after their formation. For example, single cell-encapsulating microbeads were produced by mixing poly(2-methacryloyloxyethyl phosphorylcholine (MPC)-co-n-butyl methacrylate-co-4-vinylphenylboronic acid) (PMBV) and poly(vinyl alcohol) (PVA) in a flow-focusing microfluidic device [49]. PMBV solution with HeLa cells and PVA solution were injected separately through two parallel inlets to mix them just before the formation of the droplets at the junction (Fig. 3C-i). The mixture gelled upon the reaction of the phenylboronic acid groups of PMBV with the hydroxyl groups of PVA (Fig. 3C-ii), and single HeLa cells were encapsulated within microgels with diameters of 40–80 μm (Fig. 3C-iii). Higher mass ratios of PVA in the hydrogel formulation increased the stiffness of the microgels and hindered the proliferation of the HeLa cells. In another example, single hMSCs were encapsulated in hyaluronic acid (HA) microgels crosslinked with PEG using a flow-focusing microfluidic device (Fig. 3D-i) [50]. A stream carrying cells in a mixture of thiolated HA (HASH) and fibrinogen was mixed with another stream carrying PEG divinylsulfone (PEG-DVS), and the cell encapsulating droplets were gelled into microgels of 150 μm diameter upon thiol–ene click chemistry reaction between HASH and PEG-DVS (Fig. 3D-ii). The encapsulation followed the Poisson distribution; only 30% of the microgels had single cells while the rest were either empty or with multiple cells (Fig. 3D-iii). By varying the crosslinking density, microgels with elastic modulus ranging from 0.9 to 9 kPa were obtained, and these were stable for long-term culture of hMSCs. Encapsulated cells had a rounded morphology with microscale protrusions. The viability of the encapsulated cells was 70% at 24 h after encapsulation, and some cells survived even after 4 weeks. Around half of the encapsulated cells retained multipotency at 7 days, and the cells incubated in osteogenic and adipogenic bipotential differentiation medium exhibited adipogenesis over 14 days of culture. This observation was explained with the stiffness range of the microgels being below that required for osteogenesis.

Alginate (AL) has been the most widely used hydrogel material for the microfluidic-based encapsulation of single cells. AL droplets emulsified in oil phase are ionically crosslinked with divalent cations such as calcium or barium ions. The pre-hydrogel solution gels rapidly upon contact of the AL chains and divalent cations, and the cells are trapped within the microgel [51]. For example, individual Jurkat cells were encapsulated in AL microgels produced in a flow focusing droplet microfluidic system with PDMS as the oil phase (Fig. 3E-i) [52]. Initially, a T-junction approach was studied, but the cell medium was wetter on the PDMS walls than water, hindering the formation of discrete droplets (Fig. 3E-ii). The concentration of the cells was kept relatively low and the flow rates of the aqueous and oil phases were optimized for small droplet sizes to ensure the encapsulation of only single cells (Fig. 3E-iii). The flow-focusing microfluidic device was coupled with a single-needle

bioelectrospraying (BES) system and the cell-laden AL droplets were jetted into a $CaCl_2$ bath for crosslinking. The live/dead assay of the AL encapsulated cells showed high cell viability and cellular mitosis rate, comparable with the control group.

Several other approaches, other than using a Ca^{2+} bath, have been reported for the ionic crosslinking of alginate droplets, including the production of $CaCl_2$ and AL droplets separately and merging them through the microchannels for ionic crosslinking [38]. The microfluidic device had two flow focusing setups in parallel, one producing AL droplets with human HCT116 colon cancer cells and the other producing $CaCl_2$ droplets (Fig. 4A-i). Once the cell-AL and $CaCl_2$ droplets merged, disk-shaped microgels formed instantaneously and the cells were entrapped within the AL capsules (Fig. 4A-ii). A series of microgel sizes were obtained by changing the oil flow rate, and the number of cells per droplet decreased with decreasing microgel size. About 80% of the cell-encapsulating droplets had single cells when the droplet diameter was set to ~50 μm. The viability of the encapsulated cells, however, was relatively low, with only 50% of the cells encapsulated in AL microgels with diameters of 34 to 53 μm alive.

The use of a Ca^{2+} bath or separate $CaCl_2$ droplets dilutes the AL concentration in the final microgel and reduces material stiffness. Mixing AL and Ca^{2+} is also not practical because of the rapid gelation, which may clog the microchannels and result in heterogenous, non-spherical microgels. To solve this issue, Tan and Takeuchi proposed internal gelation [53], in which water-insoluble $CaCO_3$ nanoparticles were used as the calcium source in the AL solution. $CaCO_3$ nanoparticles were solubilized by reduction of pH upon diffusion of acetic acid from the oil phase to the droplets, which released calcium ions for rapid crosslinking of AL chains. Akbari et al. modified this technique for the microencapsulation of single 9E10 hybridoma and M6C mouse breast cancer cells [54]. To prevent early interactions between the cells and potentially cytotoxic $CaCO_3$ nanoparticles, a stream carrying cells in AL solution was mixed with a second stream carrying $CaCO_3$ nanoparticles in an AL solution at a second flow-focusing junction just before the droplet formation (Fig. 4B). The concentration of AL in both streams was the same to keep AL concentration constant in the droplets. Acetic acid was used in stoichiometrically equal amounts with $CaCO_3$ to prevent extreme drops of pH within the droplets. Cells were successfully encapsulated within the AL microgels with a diameter as small as 26 μm. After encapsulation and washing steps, 84% of 9E10 cells and 86% of M6C cells were viable. The long-term viability of encapsulated M6C cells was 74% at Day 2 and 84% at day 6, indicating proliferation of the cells within the AL microgels over 6 days of culture.

Another approach used for the introduction of Ca^{2+} into the single cell encapsulating AL droplets was the use of a calcified oil phase, in which diffusion of $CaCl_2$ from the carrier oil to the aqueous droplets initiated hydrogelation. An additional channel was also coupled to the flow-focusing microfluidic setup for the introduction of $CaCl_2$ suspended in oleic acid to the cell-AL droplets (Fig. 4C-i). Individual mammalian cancer cells MCF–7, HepG2, and U937 were successfully encapsulated in AL microbeads using this device [55]. The diameter of the oil-suspended microcapsules decreased over time due to water evaporation (Fig. 4C-ii), which might reduce the viability of encapsulated cells due to dehydration. Microgels suspended in aqueous media, on the other hand, were stably maintained without significant

change in diameter during 30 min incubation. The long-term viability of MCF-7 cells in AL microcapsules was tested and the cells were viable, proliferating and formed aggregates after 6 days of culture.

In response to the approaches utilized by Akbari et al. [54] and Lee et al. [55], Weitz and co-workers argued that the use of insoluble calcium salt nanoparticles or delivery of calcium in the oil phase might cause heterogenous distribution of calcium ions in the droplets and diminish the homogeneity of the microgels. Therefore, they proposed the use of water soluble Ca- Ethylenediaminetetraacetic acid (EDTA) complexes directly in the aqueous phase, together with AL and cells. Calcium ions were expected to initially remain inaccessible to the AL chains and would be released upon diffusion of acetic acid from the oil phase into the droplets to trigger droplet gelation (Fig. 4D-i) [51]. Using this strategy in a flow-focusing microfluidic device, single hMSCs were encapsulated within RGD tripeptide-conjugated AL microgels. The size of the microbeads obtained was a function of the size of droplet forming channel and the flow rate of the oil phase. Monodisperse microbeads with a diameter in the range of 10–50 μm were obtained by adjusting these parameters. Only 25% of the microgels encapsulated single cells, while 70% of the droplets were empty (Fig. 4D-ii). The microbeads were supplemented with fibrinogen and the cells maintained a spherical shape after encapsulation. Cell viability depended on the acetic acid concentration in the oil phase and the crosslinking time, and optimization of the system led to a survival rate up to 83%.

The common problem of the studies summarized above was the low yield of cell encapsulation. The control of the average number of cells per droplet has been approached by adjusting the concentration of the cells in the hydrogel precursor solution, the flow rate of the hydrogel solution or the size of the droplets. To obtain single cells per droplet, researchers optimized these three parameters to fit the encapsulation process to Poisson statistics (Equation 4) that governs random encapsulation:

$$P(n) = \frac{\lambda^{n} e^{-\lambda}}{n!} \quad (4)$$

where P(n) is the fraction of droplets containing n cells, and λ is the average number of cells per droplet. Therefore, the cell concentration in the hydrogel solution was generally kept low to avoid encapsulation of multiple cells. This resulted in a large proportion of empty droplets [24, 30, 41]. For example, if only 1 droplet out of 100 droplets was desired to have 2 cells, 13 droplets would have single cells and 86 droplets would be empty. The most straightforward approach that has been used to increase the yield of single cell encapsulation has been fluorescence-activated cell sorting (FACS) of cell-laden of microgels. An example was reported by Kamperman et al., who encapsulated hMSCs or bovine chondrocytes in UV crosslinked polyethylene glycol diacrylate (PEGDA) microgels with diameters of 35 to 40 μm using a flow-focusing microfluidic device [39]. The stability of the water/oil interface was improved by including a photoinitiator in the oil phase as well as the aqueous phase to prevent coalescence of the droplets or escape of the cells from the microgels during crosslinking. Even though cell viability after encapsulation was over 70%, most of the

microgels were empty and the yield of single cell encapsulation was only around 10% (Fig. 5A-i). The yield was increased to over 90% by fluorescent labeling of the cells and sorting the microcapsules with single cells using FACS (Fig. 5A-ii).

Another approach to increase the fraction of single cell encapsulating microgels over empty capsules was reported by Mao et al., who limited the crosslinking of AL only in cell-laden droplets by pre-coating the cells with calcium carbonate ($CaCO_3$) or barium carbonate ($BaCO_3$) nanoparticles (Fig. 5B-i) [56]. The adsorption of the nanoparticles on the cells was carried out at 4°C to reduce endocytosis, and no significant reduction in viability was observed. After removing excess nanoparticles, pre-coated mouse MSCs (mMSCs) or OP9 pre-adipocyte cells were mixed with RGD-conjugated AL or AL/collagen (Col) blends, and the pre-hydrogel droplets were produced using acidified oil phase in a flow-focusing microfluidic system. Cell concentration was kept low to ensure encapsulation of single cells. Therefore, encapsulation followed a Poisson distribution, resulting in many empty droplets. Upon diffusion of acetic acid from the oil phase into the droplets, Ca^{2+} or Ba^{2+} ions were released, and the cells were trapped within alginate microgels upon rapid crosslinking (Fig. 5B-ii). The strategy provided a single cell encapsulation yield of over 80%, which was comparable with FACS sorting and more than 8 times higher than cell encapsulation with direct injection of the nanoparticles into the pre-hydrogel solution (Fig. 5B-iii). Unlike FACS sorting, however, microgels with multiple cells could not be eliminated completely, but their fraction was significantly lower compared to the single cell-laden particles. Both mMSCs and OP9s were encapsulated successfully in microgels with a diameter as low as 27 μm, and their viability was over 70% at 1 or 3 days after encapsulation.

The same approach was also utilized with a different hydrogel material and crosslinking mechanism. This time, Ca^{2+} was used as the cofactor of the enzyme transglutaminase factor XIII (FXIII), which catalyzed the crosslinking of star shaped PEG molecules (Fig. 5C-i). To achieve this, arms of the star-shaped PEG-vinylsulfone were modified with complementary FXIII substrate peptides [57]. The donor sequence was designed to contain a matrix metalloproteinase (MMP)-sensitive linker or RGD peptide to allow the cells to degrade the encapsulating matrix over time and provide free cell recognition sequences in the hydrogel matrix, respectively. A microfluidic device with two cross-junctions was used for the formation of cell-laden droplets. The streams of matrix precursor solution with HCl and EDTA, suspension of hMSCs pre-coated with $CaCO_3$ nanoparticles, and FXIII solution were joined at the first cross-junction. Since the optimal temperature for FXIII activity is 37°C, all solutions were kept at 4°C to prevent premature gelation before droplet formation. At the second cross-junction, droplets were formed in a fluorinated oil phase. EDTA was included in the system to bind to background Ca^{2+} and its concentration was optimized to prevent the gelation of empty droplets without significantly interfering with FXIII activity. The droplets collected in the oil phase were brought to 37°C to activate FXIII and initiate the crosslinking reaction. Over 90% of the microgels encapsulated single cells (Fig. 5C-ii). Despite the high yield of single cell encapsulation, only 20% of the cells remained in the microgels at 3 days after encapsulation. This observation was explained with the cells initially being positioned at the edge of the microgels (Fig. 5D-i). To reposition the cells in the microgels, aqueous droplets were shaken at 1000 rpm during the gelation at 37°C, and the encapsulated cells were positioned to the center (Fig. 5D-ii), which prevented their escape and significantly

increased the fraction of encapsulated cells to over 95% at day 3 and 75% at day 7 of culture.

The importance of positioning cells in the center of microgels was highlighted also by Kamperman et al., who stated that cells positioned at the edge of the microgels were more exposed to chemical, mechanical, and immunological stresses [58]. The reason of the cell positioning at the water/oil interface was hypothesized to be rapid crosslinking. Therefore, delayed crosslinking of the droplets was proposed to provide more time for repositioning of the cells in the center. This hypothesis was tested using a hydrogel system composed of tyramine conjugated dextran (Dex-TRA) or a 1:1 mixture of Dex-TRA and tyramine conjugated hyaluronic acid (HA-TRA). Tyramine conjugated polymer chains were covalently crosslinked via tyramine–tyramine bonds formed by horseradish peroxidase (HRP) in the presence of hydrogen peroxide (H_2O_2). To delay the crosslinking of hydrogel precursor, a flow-focusing microfluidic device enabled the controlled diffusion of H_2O_2 into the droplets. A PDMS device with three parallel channels was constructed: the one in the center carried the droplets of polymer-TA with HRP formed by a flow-focusing microfluidic system, and the ones on the sides carried the H_2O_2 solution in the opposite direction (Fig. 5E-i). The researchers took advantage of PDMS walls being permeable to H_2O_2, and the gelation of the droplets was delayed as H_2O_2 molecules slowly diffused through the walls into the central channel. Encapsulated hMSCs were well-centered (Fig. 5E-ii), and only 5% of the cells escaped at 7 days of culture, while this was over 25% for the cells encapsulated via direct injection of H_2O_2 into the hydrogel precursor. The viability of encapsulated MSCs was over 90%, and 80% were metabolically active at the 28 days of culture.

2.2. Nanoencapsulation

Nanocoating of mammalian cells was first proposed for the construction of artificial pancreases by nanocoating of Langerhans islets via electrostatic layer-by-layer deposition of polyelectrolytes [25–27] or covalent conjugation of polymer chains onto the modified cluster surfaces [28, 29]. Efficient transfer of nutrients and gases trough nanolayers and the relatively constant total volume of nanocoated cells have then made nanoencapsulation of single mammalian cells a favorable strategy to preserve cell viability and function [11]. Here we classify the different approaches utilized toward this goal as: deposition of nanolayers on cell surface by electrostatic interactions, receptor-ligand binding, nonspecific interactions, and cell surface modification (Table 2).

2.2.1. Deposition by Electrostatic Interactions—Deposition of polyelectrolytes and minerals on the cell surface has been the most widely employed method for nanoencapsulation of mammalian cells. Negatively charged head groups of membrane phospholipids such as phosphatidylserine [59], together with membrane glycosaminoglycans rich in sialic (N-acetylneuraminic) acid [60–62] provide a net negative charge to the mammalian cell surface under physiological conditions (Fig. 6A-i) with a zeta potential of −19 to −32 mV [63, 64]. Incubation in relatively high concentrations of positively charged substrates leads to their adsorption on cell membrane, followed by neutralization and subsequent charge reversal of the cell surface (Fig. 6A-ii, iii). The nanolayer formed is stable even after centrifugation and washing, allowing the deposition of a negatively charged

substrate as the second layer. Alternation of surface charge through successive incubations in polycation and polyanion solutions provides layer-by-layer (LbL) deposition of nanolayers (Fig. 6B), the composition, layer number and thickness of which can be tuned. This approach has been widely employed for nanocoating insulin-producing pancreatic β-islands with polyelectrolytes to protect against *in vivo* immune attack upon transplantation [65–67]. The method was then utilized on single sacrificial cells such as fixed platelets as a proof of concept for the nano-organization of polymeric layers on single cells [68, 69].

During the last decade, LbL deposition by electrostatic interactions has been of increasing interest for the nanocoating of single living mammalian cells. Synthetic polycations (Fig. 7A) such as poly(L-lysine) (PLL), polyethyleneimine (PEI) and poly(diallyldimethyl ammonium) chloride (PDDA) have been linked with synthetic or natural polyanions for layer-by-layer deposition on the cell surface. An example was reported by the Mills group [70], who demonstrated successful encapsulation of mMSCs within multiple bilayers of PLL and HA nanolayers. The adsorption of each layer was monitored by zeta potential measurement, and a net positive and negative charge was recorded after each PLL and HA step, respectively. A discrete polymer layer was observed on the cells coated with fluorescein isothiocyanate (FITC) labeled PLL on day 3, but this layer diffused into the cells on day 7 (Fig. 7B), likely because of endocytosis, indicating the loose structure and short sustenance period of the polyelectrolyte shell. The decrease in viability of nanocoated mMSCs was insignificant over 7 days of culture, while the metabolic activity decreased gradually from day 1 to 7. The type of the solvent used for LbL coating, deionized water, 0.5 M NaCl solution or Hank's Balanced Salt Solution (HBSS), did not significantly influence cell viability. In another study, human T-lymphocyte Jurkat cells coated with double bilayer shells of PLL and fullerenol-conjugated PEI displayed similar levels of metabolic activity with control cells at 8 days of culture and showed high viability after 2 weeks of encapsulation [71]. In a more recent study, PLL was coupled with either RGD tripeptide or HA for the LbL electrostatic deposition of polymer nanolayers on the surface of individual hMSCs [72]. Positively charged PLL assembled on the plasma membrane and formed a stable layer. The fluorescent intensity of the FITC labeled polyelectrolyte nanofilms increased with increasing numbers of layers deposited (Fig. 7C), indicating that successful LbL deposition was achieved by the electrostatic interactions of PLL with the negatively charged RGD and HA at the physiological pH of standard culture media. The size and round morphology of MSCs in suspension maintained after the nanolayer deposition process.

Despite the above findings regarding cell viability, the cytotoxicity associated with the deposition of polycations such as PLL and PEI on mammalian cells has been a major concern. The positive charges disrupt the integrity of negatively charged plasma membrane. The magnitude of polycation cytotoxicity was shown to depend on the molecular weight, charge density, and concentration of the polycation, as well as the incubation time [73]. The influence of several synthetic polycations and coating buffers on the viability of human breast cancer MELN cells was investigated and the type of polycation and the composition of buffer used directly affected cell viability [74]. Among the polycations used, PDDA displayed the lowest cytotoxicity compared to PLL, poly(allylamine hydrochloride) (PAH), protamine sulfate (PS), polyphosphoric acid (PPA) and PEI, even at higher molecular weight and concentration. α-PLL was cytotoxic; the viability of the cells coated with multiple

bilayers of PLL and poly(sodium 4-styrene sulfonate) (PSS) was significantly lower than those coated with PDDA/PSS, and cell viability decreased gradually with an increasing number of deposited layers. The ionic composition of the buffer used for LbL deposition also affected cell viability (Fig. 7D). The fraction of viable cells coated with four bilayers of PDDA/PSS in a buffer with K^+ ions was higher than the one with Na^+, while the presence or absence of divalent cations Ca^{2+} or Mg^{2+} did not influence cell viability. The positive effect of K^+ ions was suggested to be because of its higher binding constant to polyelectrolytes, reducing the interactions between the cell surface-polycation and polycation-polyanion and leading to a thicker, more relaxed shell conformation with less mechanical tension applied on the plasma membrane. Akashi and co-workers also reported significantly higher cytotoxicity of α-PLL over PDDA on L929 murine fibroblast monolayers (Fig. 7E), even at low concentrations [76]. This observation was explained with the ring system of PDDA that makes it harder to attach onto the cell surface due to sterical hindrance. ε-PLL, with a lower molecular weight and iso-electric point than α-PLL, displayed much lower cytotoxicity. Unlike the report by Germain et al. [74], the presence of Ca^{2+} in the incubation buffer decreased the cytotoxicity of all polycations, likely because of a reduction in electrostatic aggregation on the cell membrane.

Besides synthetic polycations, biocompatible and biodegradable natural polycations such as GL (type A) and chitosan (CH) have also been used for nanocoating individual mammalian cells. An early example included the LbL deposition of glycol-CH and poly(L-glutamic acid) (PLG) on the surface of living rabbit platelets and formation of a smooth nanoshells on the cells [76]. Researchers aimed to nanoencapsulate platelets without activating them to preserve their biofunctions. Attempts of LbL deposition using synthetic polycations PLL, PAH or PEI with with polyanions PSS or chondroitin sulfate (CS) resulted in platelet activation and caused cell dissolution during the nanocoating process. Deposition of two, three or four bilayers of glycol-CH/PLG, on the other hand, preserved the internal structures and contents of the cells, indicating successful nanoencapsulation without activation. In another study, Li et al. compared the viability of human neural stem cells (hNSCs) incubated with natural polycations GL (type A), CH, PLL and PEI, and selected GL because of its significantly lower cytotoxicity with cell viability over 90% (Fig. 7F-i) [77]. Cells were LbL coated with GL/AL bilayers (Fig. 7F-ii) and no significant reduction was recorded in their metabolic activity throughout 6 days of culture. Visualization of cells encapsulated with fluorescently labeled polyelectrolytes revealed a decrease in fluorescence from days 1 to 10, and the spread area of coated cells increased from day 1 to 7 (Fig. 7F-iii-v), indicating the degradation and break down of the nanocoat over time. The potential application of LbL nanocoats as a drug carrier was also studied. The AL solution was loaded with insulin-like growth factor-1 (IGF-1) and the polyanion layers on the cells carried IGF-1, which was released slowly in a pH-dependent manner and enhanced the proliferation of coated cells. In a more recent study by the same group, GL type A and HA bilayers were deposited as nano-thick hydrogel layers on the surface of rat PC12 cells without significantly compromising their viability [4]. The nanoencapsulation process hindered cell proliferation, and the rate decreased with increasing polyelectrolyte concentration or the number of layers deposited. The stability of the GL/HA nanocoats depended on the pH; nanolayers vanished at pH 3.0, 9.0 and 11.0 likely because both polyelectrolytes had the same charge at very low and high

pH values and the electrostatic interactions between the layers diminished. In another study, CH/AL bilayers were LbL deposited on mouse T cells and a porous nanocoat rather than an impermeable shell was obtained on the cell surface (Fig. 7G) [5]. No significant reduction in the viability of the cells was recorded, and they retained their ability to bind to antibodies, recognize and lyse tumor cells, or secrete cytokines. The proliferation of the cells in response to interleukin-2 (IL-2) stimulation was not affected by the encapsulation process, pointing to a loose layer formed around the cells that breaks apart easily during cell division.

In addition to use of pristine synthetic or natural charged polymers, several research groups have utilized polyelectrolytes that were chemically or physically modified to improve the performance or to introduce new functionalities to the nanoshells encapsulating the cells. For example, CH was chemically conjugated with phosphorylcholine groups (CH-PC) to increase solubility in water at neutral pH, and PLL was conjugated with PEG (PLL-PEG) to reduce its cytotoxicity for electrostatic deposition on human red blood cells (hRBCs) [78, 79]. The use of PLL-PEG as the first layer was still cytotoxic on RBCs, resulting in the lysis of more than 65% of the cell monolayers. Therefore, CH-PC was used to prime LbL nanocoatings of RBC membranes [78]. After optimization of cell density and polyelectrolyte concentrations, 4 bilayers of CH-PC/AL were deposited on suspended hRBCs as the internal shell, followed by 2 bilayers of PLL-PEG/AL as the external shell and a single layer of AL. Centrifugation caused aggregation and death of intrinsically fragile RBCs, therefore membrane filtration was utilized for LbL process. This approach significantly decreased aggregation and flocculation of RBCs compared to centrifugation. The polyelectrolyte nanoshells allowed oxygen uptake and preserved the viability of the RBCs [79].

An interesting polyelectrolyte modification was the coupling of the polycation with magnetic nanoparticles to encapsulate mammalian cells within a magnetically responsive nanoshell. The Fakhrullin group synthesized superparamagnetic iron oxide nanoparticles (SPIONs) and stabilized them in aqueous media by coupling with the polycation PAH that was successfully deposited on individual HeLa cells (Fig. 8A-i) [80]. As a proof of concept, HeLa cells were incubated with positively charged SPION-PAH complex and encapsulated within a uniform layer of magnetic nanoparticles via electrostatic deposition (Fig. 8A-ii,iii). Unlike cell surface labeling with magnetic nanoparticles using antibodies, aptamers, or polypeptides, SPION-PAH complex did not to pierce the cell membrane and accumulate in the cells. Most of the encapsulated cells were viable and able to colonize surfaces over time by dividing after breaking up their magnetic shells. Coated cells were magnetically responsive and could be spatially moved and collected using a permanent magnet (Fig. 8A-iv). The technique could be used to deposit various nanoparticles to improve the mechanical properties of the shells or to introduce other functionalities, such as drug release or whole-cell biosensors.

A recent study by Chen and co-workers showed that the polymeric materials with insufficient or no charged groups could be chemically modified with charged residues for LbL electrostatic deposition [11]. GL type A (GL-A), a natural polymer that has a weak positive charge at physiological pH, was enriched with amine groups through the EDC/NHS reaction of its carboxylic acid groups with ethylene diamine. Modified GL-A was coupled with negatively charged GL type B (GL-B), and GL-A/GL-B bilayers were deposited on the

surface of individual HeLa cells. Polyelectrolyte bilayers were then encapsulated with a PEG outer layer: first, thiolated 4-arm PEG conjugated GB was electrostatically deposited on previous GL-A layer. Then, maleimide-conjugated 8-arm-PEG was crosslinked on the surface via the Michael addition reaction between thiol and maleimide groups (Fig. 8B-i). After the LbL assembly process, viability of HeLa cells was determined to be over 80%, which gradually dropped below 60% over 72 h of culture. During this period, encapsulated cells failed to adhere, spread or divide on the culture plate, and the fluorescence intensity of the fluorescently labeled GL layers decreased very slightly (Fig. 8B-ii), indicating a stable nanocoating formed on the cells (Fig. 8B-iv). On-demand degradation of the nanoshells was achieved by the reduction of succinimide thioether linkages using glutathione (GSH). After the cleavage of PEG outer layer and gradual degradation of GL bilayers, cell division was recovered, and the number of cells started to increase at 2 days after release.

2.2.1.1. Biomineralization: In nature, some unicellular algae display rigid mineral cell walls that provide distinct advantages against environmental stress. The unicellular algae coccolithophores, for example, are covered with a calcium carbonate shell called a coccolith, which protects the cells from UV radiation by backscattering and reflecting UV light. Another group of microalgae called diatoms have a siliceous cell wall, which provides protection against turgor pressure and predators [81]. These structures in nature have inspired several research groups to mimic mineralized nanoshells on individual animal cells to protect them from harsh environmental conditions. Unfortunately, the lipid membranes of animal cells lack biomineralization-inducing components such as coccolith-associated polysaccharides (CAPs) rich in uronic acid with carboxylates [82] or silaffin protein of diatoms rich in lysine residues with primary amines [83]. Therefore, deposition of a priming layer on cell surface via electrostatic interactions was needed prior to nucleation of mineral layers.

One of the earliest examples of mineral deposition on individual animal cells was reported by the Tang group [84], who coated the eggs of zebrafish (Fig. 8C-i) with a nanolayer of lanthanide phosphate ($LnPO_4$) enriched with cerium (Ce^{3+}) and terbium (Tb^{3+}). First, the yolk sac of the eggs was LbL coated with three bilayers of CH/poly (acrylic acid) (PAA) to introduce carboxylic acid residues required for the nucleation of $LnPO_4$ layer. A porous, ~500 nm thick mineral capsule was formed around the eggs (Fig. 8C-ii) and 95% developed into healthy larvae without any abnormalities, indicating no negative effects on the eggs caused by the polyelectrolyte or mineral layers. Later, a similar approach was employed to nanoencapsulate individual mammalian cells within mechanically durable silica shells [85]. To create a layer suitable for the nucleation of negatively charged silicic acid into silica, surfaces of HeLa cells, NIH3T3 fibroblasts and Jurkat cells were coated with PEI. PEI, a polycation that has been considered cytotoxic, was cytocompatible with HeLa cells with over 95% of the cells primed with PEI metabolically active. After the deposition of the silica layer, the survival rate of HeLa, fibroblasts and Jurkat cells were 76%, 80% and 50%, respectively. Unlike uncoated HeLa cells that attached and grew flat on the culture plate, silica coated cells had a spherical shape (Fig. 8D) and could not attach or proliferate 12 h after encapsulation. This observation was explained with the nondegradable, mechanically tough silica layer, which masked the adhesion molecules on the cell surface and inhibited the

division of cells. Another study by the same group demonstrated the nanoencapsulation of Jurkat T cells (Fig. 8E-i) within durable titanium oxide (TiO_2) shells via electrostatic deposition [10]. For the nucleation of TiO_2 on the cell surface, a priming peptide was used. The phage-displayed Ti-1 peptide derived sequence $(RKK)_4$ was coupled to eight aspartic acid residues (D_8) to reduce its cytotoxicity by decreasing the density of positive charges [86]. After the deposition of ten $(RKK)_4D_8$ /TiO_2 bilayers on their surface, Jurkat cells were able to divide and secrete IL-2 upon induction by anti-CD3 and anti-CD28 antibodies, revealing that the peptide-mineral composite shell had a flexible, porous structure (Fig. 8E-ii) that allowed access of antibodies to the surface antigens.

2.2.2. Deposition by Receptor-Ligand Interactions—Another strategy utilized for the nanoencapsulation of individual cells in suspension involves the deposition of layers through surface receptor – ligand interactions (Fig. 9A). One of the early examples of this technique was reported by the Akashi group for the construction of multilayered cellular architectures [87]. Nanometer-thick extracellular matrix (ECM) films composed of fibronectin (FN) or laminin (LN) and GL were formed on the surface of cell monolayers and subsequent cell monolayers were LbL deposited onto the cell adhesive ECM coating of previous monolayer. Even though fibronectin and GL type B possess a net negative charge at physiological pH, RGD sequences of FN or LN and GFOGER sequence s of GL were recognized by the cell surface integrins [88], leading to their deposition on cell surface. Moreover, the intrinsic Col binding domains of FN and LN allowed for the LbL deposition of bilayers. The same method was later adapted for the encapsulation of single cells in suspension. Unlike polycations deposited via electrostatic interactions, negatively charged ECM nanofilms were cytocompatible and protected the cells against the mechanical stress created during centrifugation steps of LbL processing better than the polyelectrolyte shells. For example, the viability of single human hepatocellular carcinoma (HepG2) cells LbL coated with five bilayers of FN/GL (Fig. 9B-i, ii) [89] or Col type IV (Col-IV)/LN [9] were 91% and 89%, respectively, and the coated cells adhered and proliferated on culture plates. LbL coating with ECM-derived polymers preserved cell viability during the encapsulation process much better than the deposition of polylelectrolytes (Fig. 9B-iii). In a more recent study, centrifugation steps were omitted from the process to remove the mechanical stress created during LbL deposition. Instead, cells were collected and rinsed after the deposition of each layer using a filtration membrane, which was reported before by the Tabrizian group for the LbL nanocoating of RBCs [79]. Using this technique, FN/GL bilayers were successfully deposited on induced pluripotent stem cell-derived human cardiomyocytes (iPSC-CMs) and rat neonatal CMs [90]. The filtration method provided higher yields even at low initial cell numbers and caused less damage to the cell membrane determined by reduced leakage of cytosol molecules after the deposition of 9 layers compared to centrifugation.

Deposition of matrix molecules on individual cells was also reported through interaction with surface receptors other than integrins. For example, the Hong team took advantage of HA binding to CD44 as well as Col-integrin interactions to nanocoat rabbit MSCs [3]. Col type I (Col-I)/HA bilayers were formed on the cells via Van der Waals and weak electrostatic interactions between the slightly positively charged Col-I and negatively

charged HA. A considerable portion of the plasma membrane, however, was naked on TEM images, and no significant difference was recorded in the attachment capacities of uncoated and coated cells.

In addition to LbL deposition through binding of FN, LN or HA to Col, single cells were also encapsulated via integrin-induced self-assembly of Col molecules on the cell surface. Akashi and co-workers exploited the re-assembly of Col-I triple helices into microfibrils when the acidic pH was brought to neutral [91]. Micrometer-thick layers were deposited on human dermal fibroblasts (Fig. 9C) upon binding of Col to $\alpha_2\beta_1$ integrins and neutralization of solution pH. Cell density, Col concentration and temperature were important for deposition on cell surfaces and were optimized to prevent formation of Col aggregates or inhomogeneous layers on the cells.

A self-assembling hydrogel system selectively-deposited on platelets was reported for the inhibition of *in vitro* platelet aggregation. Naphthalene (Nap) conjugated tripeptide phenylalanine- phenylalanine-glycine (Nap-FFG) bound strongly to the surface of platelets through interactions with an unknown receptor, forming a thin layer of hydrogel [92]. The hydrogel layer surrounding the cells increased the zeta potential of the platelets because of the net negative charge of the free C-terminal carboxylic acid groups of the tripeptides. This negative charge created a strong repulsion force between the individual platelets and prevented aggregation induced by adenosine diphosphate (ADP), Col, thrombin, and arachidonic acid (AA).

2.2.3. Deposition by Nonspecific Interactions—Besides polyelectrolytes and ECM-based macromolecules, materials that are deposited on substrate surfaces through nonspecific interactions were also utilized for the nanoencapsulation of individual cells. These materials include plant-derived tannic acid (TA) and pyrogallol (PG), which display material-independent affinity to surface of nonliving objects. Choi and co-workers reported the deposition of TA and PG on the plasma membrane for the nanoencapsulation of single cells. The binding of the galloyl groups of TA to Fe(III) ions was utilized to form a nanolayer of metal-organic complex (Fig. 9D-i) on the surface of HeLa, NIH3T3 fibroblast, Jurkat [93] and red blood cells (Fig. 9D-ii, iii) [94]. The thickness of the nanofilms depended on the number of layers deposited and the concentration of Fe(III) ions, but not TA. Fe(III) ions were cytotoxic at high concentrations, therefore the concentration was optimized to obtain a stable nanofilm on the cells with highest viability. The proportion of the viable HeLa cells after coating dropped from 97% to 57% from day 1 to day 4. The TA-Fe(III) coating inhibited attachment, spreading and proliferation of the cells over 4 days of culture. Dissociation of the nanolayers upon chelating Fe(III) ions by EDTA allowed cells to adhere to the culture plate and start growing. RBCs coated in isotonic 0.85% NaCl solution maintained their original spherical shape without hemolysis or aggregation. No significant change was recorded in the oxygen consumption or capacity of RBCs after encapsulation within a 20 nm thick TA-Fe(III) shell. PG likely oligomerized on material surfaces via autooxidation of the phenolic moieties. Thus, no metal complexation was required to form PG nanolayers on the surface of HeLa cells (Fig. 9E-i, ii) and hRBCs [95]. The coating process was carried out in an isotonic solution at pH 7.8 to obtain uniform layers of PG on the cells without significant decrease in cell viability. Unlike TA-Fe(III) coated HeLa cells,

PG coated HeLa cells adhered to culture plates and proliferated even though their spherical shape was maintained to some degree. The PG coating slowed down the oxygen uptake rate of RBCs compared to native cells, possibly because of retarded O_2 diffusion through hydrophilic PG layers. The overall capacity for oxygen uptake, however, was not affected significantly, indicating that hemoglobin function was preserved.

2.2.4. Deposition by Cell Surface Modification—When the material of interest did not show a specific or nonspecific affinity to the cell membrane, the general approach was the introduction of specific agents to the cell membrane to mediate the deposition of the material. Cell surface engineering through covalent modification, physical association, hydrophobic insertion into plasma membrane, and orthogonal strategies such as genetic and metabolic engineering have been of interest for the modulation of function and interactions of cells [96]. Among them, covalent modification of membrane proteins and hydrophobic insertion into the membrane have been utilized for the nanoencapsulation of single mammalian cells.

An example of covalent modification for single cell encapsulation was reported by Yang et al., who covalently modified membrane proteins for the *in situ* polymerization of a thin layer on the cells [97]. First, N-termini of membrane proteins were acryloylated with N-acryloxysuccinimide (NAS). Acrylamide (AAm) monomers were then *in situ* polymerized on the acryloylated proteins with ammonium persulphate (APS)/N,N,N0,N0-tetramethylethylenediamine (TMEDA) initiator system. *In situ* synthesized polymer chains on the cells were crosslinked with glycerol dimethacrylate (GDMA) (Fig. 10A-i). Using this method, HeLa cells, hMSCs (Fig.10A-ii, iii) and bovine articular chondrocytes (BACs) (Fig. 10A-iv, v) were nanoencapsulated in uniform polyacrylate shells under mild conditions at physiological pH. The viability of HeLa cells was over 95% after membrane acryloylation and 85% after nanoencapsulation. This included 75% of the hMSCs and BACs and 78% of the HeLa cells shown to be metabolically active, but this dropped to around 60% 8 h after encapsulation. The crosslinked polymer shells were mechanically stable, and they inhibited the attachment and spreading of the cells on culture plates over 3 days.

In a recent study, membrane proteins were chemically modified to expose free thiol groups for the maleimide groups of the coating material to react and bind covalently [98]. The disulfide bonds of the membrane proteins on HeLa cells were reduced to thiol groups using tris(2-carboxyethyl)phosphine (TCEP) under mild conditions, and the maleimide-conjugated CS or PEG chains were reacted with these free thiol groups (Fig. 10B-i), forming a polysaccharide nanoshell encapsulating the cells (Fig. 10B-ii). Zeta potential analysis of the CS coated cells revealed a highly negative cell surface (Fig. 10B-iii) because of the acidic side groups of CS. This high surface negativity prevented the aggregation of the coated cells in suspension (Fig. 10B-iv) and allowed the construction of cell clusters in the presence of polycation PLL by bridging individual cells through electrostatic interactions (Fig. 10B-v). PEG nanolayers were also introduced onto cell surfaces by deposition of maleimide-conjugated PEG-monoacrylate. Coated cells were then incorporated into PEGDA-based macrogel solutions before crosslinking, so the cells were covalently attached to the hydrogel matrix.

The approach of hydrophobic insertion into the plasma membrane for the nanoencapsulation of single cells has been introduced by the Taya group, who pioneered the *in situ* crosslinking of hydrogels nanolayers on the cell surface. The approach was based on the immobilization of the enzyme HRP on the plasma membrane to restrict the crosslinking of polymer chains with phenyl groups to the cell surface (Fig. 10C-i). For this purpose, HRP was conjugated to a biocompatible anchor molecule (BAM) molecule composed of a single oleyl chain derivative coupled with hydrophilic PEG [99]. As a proof of concept, various biocompatible polymers including HA, AL, GL and PVA were enriched with phenolic hydroxyl (Ph) groups for the hydrogelation reaction. After the insertion of BAM-HRP conjugates into the cell membrane, the mouse embryonic fibroblast cell line STO, HeLa, HepG2 and human epithelial cells were incubated in a mixture of Ph-polymer and H_2O_2, and a thin layer of hydrogel was formed on their surface (Fig. 10C-ii, iii). The amount of hydrogel sheath deposited on the cells increased with increasing BAM-HRP concentration, polymer concentration and soaking time, and H_2O_2 concentration to a certain degree. When the H_2O_2 concentration was too high, hydrogel formation decreased, likely because of the deactivation of HRP. Survival rate of the nanocoated STO cells was over 90%. Unfortunately, insertion of BAM into the plasma membrane was found to induce the production and secretion of reactive oxygen species by the cells [100], limiting the strategy.

In another study by the same group, the need for BAM-HRP was bypassed using HRP conjugated antibodies against surface antigens, which provided a safer alternative and allowed for cell selective encapsulation [101]. Successful nanoencapsulation of anti-CD326-HRP labeled HepG2 cells in Ph-AL nanolayers (Fig. 10C-iv, v) confirmed the feasibility of the strategy. To emphasize cell selectivity of the method, a mixture of CD31(+) human umbilical vein endothelial cells (HUVECs) and CD31(−) mouse embryo fibroblast-like 10T1/2 cells were incubated with anti-CD31-HRP and only HUVECs were selectively coated with Ph-GL hydrogel shells. The viability of the nanocoated HepG2 was over 90% at 30 min and 24 h after encapsulation. Coated cells maintained their spherical shape and were able to spread and proliferate only after the degradation of AL hydrogels using alginate lyase. The most important advantage was that it could be employed with a large variety of polymers carrying phenyl hydroxyl moieties, such as sugar beet pectin [102], silk fibroin [103] and tyramine conjugated synthetic polymers [104].

3. Protection of Encapsulated Mammalian Cells from *In vitro* Environmental Stresses

Micro- and nanocapsules isolate single cells from their surroundings by acting as a physical barrier around the cells. In this section, protection of encapsulated cells against harsh in vitro and in vivo conditions including anoikis, UV radiation, polycations, proteolytic enzymes, antibodies, physical forces, non-culture temperatures and immune clearance are discussed (Table 3).

3.1. Protection against Anoikis

Adherent mammalian cells require the structural support and biochemical signals from their basement matrix to survive and function. Cell adhesive sequences such as the RGD

tripeptide recognized by integrins and other ECM receptors initiate intracellular signaling cascades including focal adhesion kinase (FAK) initiated MEK-MAPK-ErK and PI3K-Akt pathways, which modulate morphology, survival, migration, proliferation and differentiation of adherent cells. Therefore, the very first stress the adherent mammalian cells (particularly MSCs) experience in suspension is the lack of a matrix support, which eventually leads to apoptotic cell death called anoikis, a Greek word for “homelessness” [1–3]. Reduced cell viability due to anoikis is currently a crucial limiting factor in tissue engineering and regenerative medicine applications such as 3D bioprinting and cell transplantation therapy. Encapsulation of individual mammalian cells has been proposed as an effective method to provide matrix support to cells in suspension.

Nanoencapsulation of cells in natural ECM components such as FN, LN, Col/GL and HA provide intrinsic cell recognition signals, improving the survival of the coated cells. The influence of single cell encapsulation within nanoshells of ECM-based materials was explored through the comparison of the viabilities of native and coated cells under suspended culture conditions. For example, Choi et al. [3] cultured MSCs with and without Col/HA LbL nanocoatings in an attachment-deprived state on non-adhesive polyhydroxyethylmethacrylate (poly-HEMA) coated surfaces and the metabolic activity of coated cells was significantly higher than that of uncoated controls over 3 days of culture (Fig. 11A). This observation was explained with the survival signals provided by integrin-Col and CD44-HA interactions on the cell surface.

When the coating materials did not have intrinsic cell recognition sites, however, the strategy to provide survival signals has been the use of chemical conjugation or supplementation with ECM proteins or peptides. For example, hCSCs encapsulated in agarose-(f/f) microgels expressed higher levels of pro-survival integrins $\alpha_V\beta_3$ and $\alpha_5\beta_1$ and therefore had significantly higher viability and proliferation rates on poly-HEMA coated surfaces compared to cells in agarose-only capsules or uncoated cells (Fig. 11B) [2]. The expression of apoptotic stress-related genes Jun, Fos and Bcl-2 by the adherent cells and the cells encapsulated with agarose-(f/f) in suspension were comparable, while their expression by the uncoated cells in suspension were significantly higher due to lack of integrin mediated intracellular survival signals. Similar findings were reported for the hMSCs. Viability of hMSCs encapsulated in agarose microgels supplemented with fibrinogen and fibronectin (f/f) was significantly higher than those in agarose only microgels, when incubated in an attachment-deprived state on non-adhesive poly-HEMA coated surfaces (Fig. 11C-i). Contrary to the spherical morphology of the cells in only-agarose microgels (Fig. 11C-ii), cells in agarose-(f/f) displayed a reorganized actin cytoskeleton with filipodia-like extensions (Fig. 11C-iii) and higher phosphorylated ERK kinase. These observations indicated that (f/f) supplementation provided cell adhesion sites and provided survival signals through the integrin mediated MAPK/ERK pathway [1].

Chemical conjugation of the RGD tripeptide was also utilized for the modification of AL [56] and PEG [57] for the microencapsulation of single MSCs and OP9 cells with high viability in suspension. The survival advantages over the encapsulation with unmodified pristine material or uncoated cells was not discussed.

3.2. Protection against UV Irradiation

UV radiation is lethal for living cells since it induces mutations in photosensitive DNA and creates DNA photoproducts, causing genotoxicity and cytotoxicity [105]. In some hydrogel-based tissue engineering applications, such as the fabrication of cell encapsulating macrogels [106] or 3D-bioprinting of cell-laden patterns [107], mammalian cells are exposed to UV radiation during the photo-crosslinking of the pre-hydrogel solution, which was acknowledged to influence the viability of encapsulated cells significantly [108].

Nanocoating of single cells with UV absorbing or reflecting materials has been proposed for the protection of cells from UV irradiation during *in vitro* manipulation. For example, $LnPO_4$ shells deposited on zebrafish eggs via electrostatic deposition blocked the penetration of UV radiation by effectively absorbing UV-B (280–320 nm) to a degree comparable with the absorption by pure $LnPO_4$ particles in solution [84]. The $LnPO_4$ nanocapsule increased the viability (Fig. 11D) and hatchability of the fertilized eggs and lowered the frequency of embryonic abnormalities compared to bare eggs after long term (80h) exposure to UV-B light. Coating of living cells with materials having crystalline photonic structures was stated as a future perspective to protect the cells by backscattering the UV radiation rather than its absorption. In another study, the protective effect of TA-Fe(III) metal-organic complex nanocoat against UV irradiation was evaluated by exposing the uncoated and coated cells to UV-C (200–280 nm) rays at 254 nm [93]. TA layers that are known to absorb UV light protected the cells against short term exposure. After 5 min of exposure, more than half of the uncoated HeLa cells were dead, while more than 60% of the coated cells were alive. The viability of the cells increased with an increase in the concentration of Fe(III) ions and the number of layers deposited (Fig. 11E). The viability of the cells coated with 2 or 3 layers using 0.1 $mg.mL^{-1}$ Fe(III) ($[TA\text{-}Fe(III)_{0.1}]_3$) was 75%, while this value was 61% for $[TA–Fe(III)_{0.1}]_1$ and 51% for $[TA–Fe(III)_{0.06}]_1$. The viability of NIH3T3 fibroblasts coated with $[TA\text{-}Fe(III)_{0.1}]_3$ was over 80% but that of Jurkat cells was only 61%, indicating varying sensitivities of different cell types to UV irradiation.

3.3. Cytoprotection by Size-selective Permeability

Cytotoxic components such as chemically reactive species and polycations found in bioink solutions, and proteolytic enzymes, immune cells and antibodies available in biological fluids compromises cell viability and limits *in vitro* and *in vivo* applications of mammalian cells. Encapsulation of individual cells within protective shells has been hypothesized to prevent the exposure of the encapsulated cells to cytotoxic agents by acting as a physical barrier, while allowing for the diffusion of oxygen and nutrients [39, 97]. To confirm the size-selective protective effect of microgels and nanocoats, resistance of the encapsulated cells to polycations, proteolytic enzymes and antibodies have been investigated. For example, Leijten and co-workers studied the permeability of UV crosslinked PEGDA microgels to fluorescently labeled BSA, IgG and dextran [39]. Diffusion of the molecules depended on their size; molecules with a hydrodynamic diameter larger than 10 nm were blocked by the capsule (Fig. 12A-i) and could not diffuse into the center. The microgels were permeable to dextran (10 to 50 kDa) or BSA (66 kDa) but not to IgG (150 kDa). When microencapsulated hMSCs were cocultured with endothelial cells in fibrin hydrogels, vascular networks formed

within micrometers of the encapsulated cells, but there was no direct contact between them (Fig. 12A-ii), indicating successful isolation of hMSCs from their microenvironment.

Nanocoatings also provided size-selective permeability. For example, the diffusion of the FITC labeled dextran (FD) into the rat PC12 cells through the GL/HA bilayers was a function of the nanolayer thickness and the molecular weight of dextran [4]. FD of 4 kDa diffused more readily than FD of 40 kDa and 250 kDa, but the diffusion of each molecule was significantly retarded in the nanocoating group compared to the uncoated cells. The permeability of the nanocoats was also tested for the diffusion of tumor necrosis factor alpha (TNF-α) and Actinomycin D (ActD), which trigger apoptosis by binding to the surface receptor TNF-R1 and intracellular dsDNA, respectively. The accumulation of fluorescently labeled TNF-α on the surface of coated cells after incubation decreased by 60% on day 0 and 30% on day 3 compared to the control group, suggesting that the bilayers successfully acted as a physical barrier. The apoptosis rate after incubation in a mixture of TNF-α and ActD was significantly lower in the nanocoated group compared to uncoated control at all time points but increased gradually from day 0 to 7. Overall, the gradual increase in the fluorescent intensities of FD and TNF-α together with the apoptosis rate suggested a gradual degradation of the nanoshells, leaving the cells unprotected in time.

Polycations and proteolytic enzymes are known to cause damage in the cell membrane and reduce cell viability. The former disrupts the integrity of negatively charged cell membrane due to large number of positive charges, leading to the leakage of cytosolic components and cell lysis at high concentrations. Proteolytic enzymes, on the other hand, cleaves membrane proteins and impair their functions, disrupting membrane integrity. Nanoshells formed on individual mammalian cells were less permeable than the microcapsules, successfully blocking the diffusion of polycations or proteolytic enzymes with molecular weights less than 30 kDa. Choi and co-workers demonstrated that HeLa cells nanoencapsulated in silica [85] or TA-Fe(III) metal-organic complex [93] layers were significantly more resistant to polycations than uncoated cells. Almost 60% of the silica coated cells were viable after 1 h incubation in PAH (~25 kDa) solution, while more than 80% of the uncoated cells were dead (Fig. 12B). The protection by silica shells against polycations was explained with adsorption by the negatively charged silica layer, and the resulting charge compensation prevented further interaction of PAH with the cell membrane. Similarly, the concentration of PEI (~25 kDa) required to kill 50% of HeLa cells nanocoated with 3 layers of TA-Fe(III) was more than 10 times higher than that required to kill uncoated cells. The degree of protection increased with increasing number of layers deposited on the cells. In addition to blocking the penetration of PAH, silica nanocoating protected the cells also against proteolytic damage by trypsin (~24 kDa). More than 70% of the coated cells survived 2 hours of incubation in trypsin-EDTA solution, while the uncoated cells had a survival ratio of only around 30%. In a more recent study, HeLa cells nanoencapsulated within GL/PEG nanolayers were more resistant to the cytotoxicity of PEI or trypsin compared to the uncoated cells [11]. In this case, 61% of the encapsulated cells survived incubation in PEI for 2 h, while more than 80% of the uncoated cells were dead. Similarly, more than half of the coated cells were alive after incubation with trypsin-EDTA solution for 4 h, while only 27% of the uncoated cells survived (Fig. 12C).

Hydrogel nanolayers *in situ* polymerized on the cell surface also displayed size selective permeability and protected the cells against polycations [97]. Polyacrylamide layers encapsulating HeLa cells allowed the staining of the cells with dyes with diameters less than 10 nm such as calcein AM and WST-1. PEG coated gold nanoparticles (~80 nm), however, were not allowed to diffuse into the cells, while they were able to diffuse into and accumulate in the uncoated cells (Fig. 12D). The cytotoxic effect of PEI with a hydrodynamic diameter ranging from 5 nm to 50 nm on the uncoated and coated cells was also investigated. After 2 h incubation in PEI, the viability of nanoencapsulated cells was significantly higher than that of uncoated counterparts at all concentrations. These observations indicated that the nanocoats resisted the permeation of high molecular weight molecules or large particles.

3.3.1. Immunocamouflage—Nanoencapsulation has been an effective approach to limit the accessibility of antibodies to cell surface antigens, providing immunocamouflage to the encapsulated cells. A common practice to investigate this aspect of single cell encapsulation has been the agglutination assays of anti-A, anti-B, and anti-D (Rh) on the coated RBCs. The study by Mansouri et al. [79] was one of the earliest examples, in which electrostatic deposition of phosphorylcholine-grafted CH/AL and PLL-PEG/AL bilayers prevented the agglutination of hRBCs after antibody screen. All coated hRBCs displayed a serologic behavior comparable to group O cells while the uncoated cells agglutinated, indicating effective camouflaging of the surface antigens by the nanolayers deposited on the cells. Similar observations were reported by the Choi group, who tested the agglutination of hRBCs coated with TA-Fe(III) [94] or PG [95] (Fig. 12E) nanolayers. Encapsulated cells were unaffected from the antibodies while the native cells were harshly agglutinated, confirming that an immunoprotective barrier was formed and the surface antigens were successfully masked.

Besides RBCs, nanoencapsulated HeLa cells were also protected from recognition by antibodies (Fig. 12F). To investigate the barrier effect of nanocoatings, Chen and co-workers incubated HeLa cells nanocoated with *in situ* polymerized polyacrylamide [97] or GL/PEG [11] layers in FITC-labeled CD44 solutions. A clear fluorescent layer was observed around the native cells, while the coated cells had no fluorescent signal on their surface, indicating that the infiltration of FITC-anti-CD44 with a molecular weight of 85 kDa and hydrodynamic size over 10 nm was successfully blocked by the nanoshells.

3.4. Protection against Mechanical Stress

Cells used *in vitro* and *in vivo* applications encounter a combination of fluid and solid mechanical stresses. One of the most important benefits of single cell encapsulation is the structural support that protects the fragile plasma membrane of mammalian cells from physical forces (Fig. 13A). Researchers have investigated the mechanical resistance of encapsulated cells to a variety of physical forces to determine the shielding effect of the micro- and nanoshells.

Mechanical properties of the microgels encapsulating single mammalian cells could be modulated by adjusting polymer concentration, molecular weight, and crosslinking density.

For example, the elastic modulus of AL microgels encapsulating single mMSCs or OP9 cells was increased up to 16 kPa by increasing the molecular weight and concentration of AL, concentration of $CaCO_3$ nanoparticles adsorbed on the cells, or the concentration of acetic acid in oil phase for the solubilization of $CaCO_3$ [56]. The resistance of the softest (E=300 Pa) and stiffest (E=16 kPa) microgels to *in vitro* shear forces was tested using rheometry, and even the softest microgel withstood shear forces ten times higher than arterial pressure. This finding suggested that encapsulation in AL microbeads could successfully protect the cells from the shear stresses in the circulatory system *in vivo*.

The investigation of the protective effects of nanocoats against the extremes of mechanical forces has been of greater interest than microgels. Nanofilms of a variety of materials deposited on the surface of mammalian cells successfully preserved the integrity of encapsulated cells from mechanical stress and significantly increased cell viability compared to the native cells. PLL/RGD and PLL/HA bilayers deposited on the surface of MSCs protected the cells from continuous agitation in liquid media under an attachment-deprived state [72]. An agitation speed of around 30 cm/s was applied to native and nanocoated cells in a nonadherent tubing. The viability of the coated cells after 1 day of culture under agitation was 1-to 3-fold higher than that of the native cells (Fig. 13B).

In another study, Matsuzawa et al. demonstrated that FN/GL and Col-IV/LN bilayers not only protected HepG2 cells from centrifugal forces applied during encapsulation processes, but also from post-encapsulation centrifugation at high rotation speeds [9]. The integrity of plasma membranes during centrifugation cycles was analyzed by measuring the activity of lactate dehydrogenase (LDH) released from the damaged cells. Cells nanocoated with FN/GL or Col-IV/LN bilayers had significantly lower levels of LDH activity compared to the uncoated cells, which displayed a linear increase in the activity of released LDH over 10 cycles of centrifugation (Fig. 13C). The viability of the uncoated cells after 18 cycles of centrifugation at 2,500 rpm (required for the LbL deposition of 9 layers including washing) was only 6%, while it was over 85% for the coated cells (Fig. 13D). This trend did not change even when the centrifugation speed was increased to 10,000 rpm. The protective effect of the nanocoats depended on the shell thickness; nanofilms thicker than 5 nm resulted in cell viability higher than 85%. The physical resistance of the fully coated cells was tested by additional centrifugation after the encapsulation process. Ten more centrifugation cycles were required to decrease the viability of coated cells to 20%, while only 4 cycles were required for the freshly detached uncoated cells. These observations indicated that nanoencapsulation with ECM components preserved the integrity of the cell membrane and protected the cells from death under high centrifugal forces. A similar repeated centrifugation analysis was done by the Chen group to determine the protective effect of GL/PEG nanocoating on HeLa cells against physical stress [11]. Coated and native cells were centrifuged 6 times for 5 min at forces ranging from 110 to 3,300 g. An increase in the resistance to mechanical stress upon nanoencapsulation was reported. The viability of the coated cells was over 80% even after centrifugation at 3,300 g (6,000 rpm), while it was less than 20% for the uncoated cells after centrifugation at 360 g (2,000 rpm) (Fig. 13E).

3.5. Protection against Non-culture Temperatures

Preservation of cell viability during handling and storage under non-culture conditions is important for the in vitro and in vivo performance of the constructs. Fluctuations in temperature are one the environmental stresses that affect the performance and viability of the cells. Youn et al. tested the protection of Jurkat T cells against mild changes in temperature by nanoencapsulation of single cells in titania shells [10]. Both naked and nanocoated cells were incubated in suspension at 25°C or 40°C for 2 weeks and 6 days, respectively, and titania shells were shown to provide moderate protection against low and high temperature. More than 65% of the uncoated cells died after a week at 25°C (Fig. 14-i) or 2 days at 40°C (Fig. 14-ii), while more than half of the coated cells were viable. Viabilities of the coated cells decreased after 2 weeks at 25°C and 6 days at 40°C, but they were still higher than those of uncoated counterparts. These findings suggested that titania nanoshells provided single cells with enhanced survival under non-culture conditions.

3.6. Protection against immune clearance

Protection from anoikis and shear forces combined with the immunocamouflage provided by microgels and nanoshells (Fig. 15A) have been exploited in cell transplantation applications to increase the duration of retention in the host and improve the viability of both transplanted cells and the host. One of the earliest studies demonstrated single cell encapsulation in agarose-(f/f) microbeads as an effective approach to improve *in vivo* retention of the cells [1]. The number of microencapsulated rMSCs in Gastrocnemius muscles was significantly higher than that of naked cells at 3 days after injection into hindlimb (Fig. 15B), suggesting a retarded clearance of the microencapsulated cells. Similarly, acute retention and survival of agarose-(f/f) microencapsulated hCSCs in immune deficient mice was significantly higher than those of naked cells over 3 weeks. In myocardial infarction models, microencapsulated hCSCs accumulated in the peri-infarct and infarct regions of the scarred animals (Fig. 15C-i), and the degree of cardiac repair was significantly upregulated. The infarct size was much smaller in the microencapsulation group compared to the native cells or blank PBS solution (Fig. 15C-ii) [2]. These findings suggested that delayed clearance and longer survival of the transplanted cells provided by microencapsulation might help improve the therapeutic effects of cell transplantation.

Comparable findings were reported also by Mooney and co-workers [56], who found 10 times longer retention of microencapsulated Balb/c mMSCs in the lungs of C57/BL6 compared to uncoated cells mixed with empty AL microgels. Twenty-four hours after injection, uncoated cells were cleared from the lungs of the host while the microencapsulated cells were maintained even at 96 h after injection (Fig. 15D). Upon injection of mMSCs genetically modified to secrete Gaussia luciferase (Gluc), blood Gluc levels of the host injected with microencapsulated cells was significantly higher. Similarly, microencapsulated hMSCs injected into NOD scid gamma (NSG) mice stayed in the host 5 times longer than native cells, and displayed more than 90% viability over 72 h. The level of human IL-6 in blood plasma of the host was two-fold higher in the microencapsulation group than the control group. Overall, these findings suggested that microencapsulation enhanced donor cell retention and therefore the secretion of small molecules.

Like microgels, encapsulation in nanoshells was also reported to enhance *in vivo* performance of the single mammalian cells by protecting them from harsh body conditions. A recent example by Kim et al. demonstrated longer retention of HeLa cells in mice with normal immunity after coating with PEG nanolayers and mesoporous silica nanoparticles (MSN) loaded with the immunosuppressant dexamethasone [98]. Like PEG nanolayers, MSNs were also chemically conjugated to reduced membrane proteins via thiol-ene click chemistry. The fluorescent intensity of luciferase-expressing implanted HeLa cells was noticeably higher after 4 days in the only-PEG-coating group compared to the uncoated cells, and in PEG-coating with MSN group compared to only-MSN-coating group (Fig. 15E), indicating retardation of immune clearance by the PEG nanoshells. A synergistic effect of protective PEG shell and drug-delivering MSN was proposed as an effective approach against host versus graft attacks against transplanted cells.

In addition to protecting the encapsulated donor cells, single cell encapsulation was also able to protect the hosts from the side effects of allogeneic transplantation of immune cells and graft versus host disease (GVHD). For example, Balb/c mice injected with allogeneic T cells nanocoated with CH/AL bilayers had a lower GVDH score (calculated based on ruffled fur, fur loss, hunching, weight loss, reduced activity, [5]. Even though the nanocoating diarrhea) and lived longer than mice injected with naked T cells (Fig. 15F-i) minimized the alloreactivity of T cells, their reactivity against tumor cells was not significantly affected. Unlike Balb/c mice cells injected with only allogeneic bone marrow cells (BMCs), mice injected with both BMCs and naked or nanocoated T cells displayed no tumor growth over 70 days (Fig. 15F-ii). The viability of mice injected with BMCs and naked T cells at day 83, however, was only 20%, while it was 81% for the nanocoated T cell group. Based on these findings, researchers concluded that nanoencapsulation of T cells could be an effective approach to enhance host survival during treatment of hematopoietic malignancy by minimizing GVHD.

4. Summary and Future Perspectives

Encapsulation in micron scale hydrogel beads or the deposition of nanolayers on the cell surface has introduced a new field for the isolation of single mammalian cells from their surroundings to protect them against various *in vitro* and *in vivo* stresses. Many synthetic and natural polymers with a wide range of crosslinking strategies have been successfully employed as hydrogel systems for the microencapsulation of single cells. Meanwhile, a variety of organic molecules such as synthetic or biopolymers and inorganic materials including minerals or magnetic nanoparticles were deposited directly on the cell surface as encapsulating nanolayers through electrostatic, receptor-ligand or nonspecific interactions, or nano-thick layers of hydrogels were polymerized or crosslinked directly on the cells after corresponding modification of the cell surface. These strategies have been demonstrated on a range of mammalian cells including mesenchymal, cardiac or neural stem cells, fibroblasts, T cells, RBCs and cancer cells. Both micro- and nanocapsules have been tested for protecting the encapsulated cells against a range of harsh environmental conditions. They were found to preserve cell viability under attachment-deprived anoikis conditions or extremes of physical forces by providing structural support, and against UV irradiation, polycations, proteolytic enzymes, *in vivo* immune clearance or graft versus host attack by

acting as an effective physical barrier with size-selective permeability. Encapsulated cells can be effectively incorporated in biofabrication such as 3D bioprinting that requires preservation of cell integrity, viability and function under harsh processing conditions. A proof of concept was reported by the Leijten group with microencapsulated hMSCs in UV-crosslinked PEGDA microgels, which were incorporated in photopatterned PEGDA macrogels, emulsified dextran-tyramine conjugates, injection molded Col matrices, 3D-printed AL/GL methacryloyl (GelMA) hydrogels, and wet-spun AL hydrogels (Fig. 16) [39]. Cell viability after processing was not discussed, but encapsulated cells were distributed homogenously in all constructs irrespective of the material type or fabrication technique.

Even though single mammalian cells armored in protective shells hold promise in terms of protection against environmental stresses, there is still much to improve in micro- and nanoencapsulation strategies. For example, the long-term culture of microencapsulated cells is problematic due to the poor mass transfer through the microscale barrier that may lead to disorders in the encapsulated cells. Large volumes provided by the high polymer-to-cell ratio of the microcapsules allow the proliferation of the cells and formation of clusters, which may eventually suffer hypoxia and starvation due to the impaired transfer of oxygen and nutrients to the center. More importantly, the maximum single cell encapsulation efficiency is still below 80% due to Poisson statistics governing the random encapsulation of diluted cell suspensions into droplets. Several geometrical strategies have been developed for the encapsulation of only single cells for the microfluidics-based single cell analysis. For example, curved microchannels in the form of spirals were conjugated to regular flow-focusing microfluidic devices to introduce the Dean force, which caused the cells to focus into a single equilibrium position. A periodicity of droplet generation matched with the cell flow then allowed for significant increase in single cell encapsulation efficiency [43]. Other approaches included the inertial ordering of the cells in the aqueous stream through a relatively long microchannel between the aqueous inlet and the flow-focusing junction [41] and multi-step splitting of the cell-laden droplets through microchannels that were sequentially divided into two branch channels 3 times to form 8 parallel branches [45]. None of these strategies, however, has been employed in the microencapsulation of single mammalian cells in hydrogel beads. Utilization of these strategies may enable researchers to increase the yield of single cell encapsulation without using time consuming FACS or potentially cytotoxic nanoparticle adsorption on the cells.

Despite the efficient diffusion of nutrients and gases through the nanolayers encapsulating single cells in a relatively constant volume, nanoencapsulation strategies also has shortcomings that limit widespread applications. The cytotoxicity of synthetic or natural polycations used in electrostatic deposition of nanofilms on cell surface forces researchers to carefully optimize the molecular weight and charge density of the polycation and the content of coating buffers. The increased fragility of the cell membrane during the deposition of polycations further increases the sensitivity of the cells to the centrifugal forces, dramatically reducing their viability. In addition to the LbL deposition of nanolayers using filtration membranes employed by Mansouri et al. [79] and Amano et al. [90], a microfluidic pinball setup that was used for the LbL coating of oil droplets with polyelectrolytes [109, 110] could also be employed for the nanoencapsulation of mammalian cells. Another limitation of nanoencapsulation is the non-degradable films of synthetic materials on the cells that even

restrict the long-term attachment, spreading and proliferation of the cells. The development of cell encapsulating shells that degrade on demand is important for the proper functioning of the cells after fabrication processes such as 3D printing that require cell protection by nanocoating. Modification of the coating materials to display stimuli-responsive degradation such as the introduction of MMP [57], or chemical reduction-sensitive sequences [11] would facilitate advancement in the single cell nanoencapsulation field.

Overall, the resistance of micro- and nanoencapsulated single mammalian cells against harsh environmental conditions indicates great potential in the fields of biofabrication and cell therapy. With the investigation of the viability and functions of encapsulated cells in detail during and after biofabrication processes would reveal the advantages and shortcomings of the strategies used so far, allowing for further advancements in the field.

Acknowledgements

We thank the NIH (5P41EB002520), the Air Force Office of Scientific Research, and the Army Research Office (W911NF-17–1-0384) for support of some of our own studies related to this topic. Authors also acknowledge the Turkish Fulbright Commission for PhD fellowship (for O.H).

Abbreviations

3D	Three-dimensional
AL	Alginate
BAC	Bovine articular chondrocytes
BAM	Biocompatible anchor molecule
CH	Chitosan
Col	Collagen
CS	Chondroitin sulfate
Dex	Dextran
ECM	Extracellular matrix
EDTA	Ethylenediaminetetraacetic acid
f/f	Fibronectin/fibrinogen
FACS	Fluorescence-activated cell sorting
FITC	Fluorescein isothiocyanate
FN	Fibronectin
GL	Gelatin
GVHD	Graft versus host disease
HA	Hyaluronic acid

hCSC	Human cardiac stem cell
hMSC	Human mesenchymal stem cell
hNSC	Human neural stem cell
hRBC	Human red blood cells
HRP	Horseradish peroxidase
LbL	Layer-by-layer
LN	Laminin
MMP	Matrix metalloproteinase
mMSC	Mouse mesenchymal stem cell
PAA	Polyacrylic acid
PAH	Polyallylamine hydrochloride
PDDA	Polydiallyldimethyl ammonium chloride
PDMS	Polydimethylsiloxane
PEG	Polyethylene glycol
PEGDA	Polyethylene glycol diacrylate
PEI	Polyethyleneimine
PG	Pyrogallol
PLGA	Poly(lactide-co-glycolide
PLL	Poly-L-lysine
Poly-HEMA	Polyhydroxyethylmethacrylate
PPA	Polyphosphoric acid
PSS	Polystyrene sulfonate
PVA	Polyvinyl alcohol
rMSC	Rabbit mesenchymal stem cells
SPION	Superparamagnetic iron oxide nanoparticles
TA	Tannic acid
TRA	Tyramine

References

[1]. Karoubi G, Ormiston ML, Stewart DJ, Courtman DW, Single-cell hydrogel encapsulation for enhanced survival of human marrow stromal cells, Biomaterials 30(29) (2009). 5445–5455. [PubMed: 19595454]

[2]. Mayfield AE, Tilokee EL, Latham N, McNeill B, Lam BK, Ruel M, Suuronen EJ, Courtman DW, Stewart DJ, Davis DR, The effect of encapsulation of cardiac stem cells within matrix-enriched hydrogel capsules on cell survival, post-ischemic cell retention and cardiac function, Biomaterials 35(1) (2014) 133–142. [PubMed: 24099706]

[3]. Choi D, Park J, Heo J, Oh TI, Lee E, Hong J, Multifunctional Collagen and Hyaluronic Acid Multilayer Films on Live Mesenchymal Stem Cells, ACS Appl. Mater. Interfaces 9(14) (2017) 12264–12271. [PubMed: 28322547]

[4]. Li W, Zhang G, Guan T, Zhang X, Khosrozadeh A, Xing M, Kong J, Manipulable permeability of nanogel encapsulation on cells exerts protective effect against TNF-α-induced apoptosis, ACS Biomater. Sci. Eng, 4(8) (2018) 2825–2835.

[5]. Zhao S, Zhang L, Han J, Chu J, Wang H, Chen X, Wang Y, Tun N, Lu L, Bai XF, Yearsley M, Devine S, He X, Yu J, Conformal Nanoencapsulation of Allogeneic T Cells Mitigates Graft-versus-Host Disease and Retains Graft-versus-Leukemia Activity, ACS Nano. 10(6) (2016) 6189–6200. [PubMed: 27224853]

[6]. Berthiaume F, Maguire TJ, Yarmush ML, Tissue Engineering and Regenerative Medicine: History, Progress, and Challenges, Annu. Rev. Chem. Biomol. Eng 2 (2011) 403–430. [PubMed: 22432625]

[7]. Mao AS, Mooney DJ, Regenerative medicine: Current therapies and future directions., Proc. Natl. Acad. Sci. U. S. A 112(47) (2015) 14452–14459. [PubMed: 26598661]

[8]. Khademhosseini A, Langer R, A decade of progress in tissue engineering, Nat. Protoc 11(10) (2016) 1775. [PubMed: 27583639]

[9]. Matsuzawa A, Matsusaki M, Akashi M, Effectiveness of nanometer-sized extracellular matrix layer-by-layer assembled films for a cell membrane coating protecting cells from physical stress, Langmuir 29(24) (2013) 7362–7368. [PubMed: 23092370]

[10]. Youn W, Ko EH, Kim M-H, Park M, Hong D, Seisenbaeva GA, Kessler VG, Choi IS, Cytoprotective Encapsulation of Individual Jurkat T Cells within Durable TiO 2 Shells for T-Cell Therapy, Angew. Chemie 56(36) (2017) 10702–10706.

[11]. Yang J, Li J, Li X, Wang X, Yang Y, Kawazoe N, Chen G, Nanoencapsulation of individual mammalian cells with cytoprotective polymer shell, Biomaterials 133 (2017) 253–262. [PubMed: 28445804]

[12]. Murphy SV, Atala A, 3D bioprinting of tissues and organs, Nat. Biotechnol 32(8) (2014) 773. [PubMed: 25093879]

[13]. Wang S, Lee JM, Yeong WY, Smart hydrogels for 3D bioprinting, Int. J. Bioprinting 1(1) (2015) 3–14.

[14]. Mandrycky C, Wang Z, Kim K, Kim DH, 3D bioprinting for engineering complex tissues, Biotechnol. Adv 34(4) (2016) 422–434. [PubMed: 26724184]

[15]. Colosi C, Costantini M, Barbetta A, Dentini M, Microfluidic bioprinting of heterogeneous 3d tissue constructs, in: Methods Mol. Biol 28(4) (2017) 677–684.

[16]. Zhang YS, Yue K, Aleman J, Mollazadeh-Moghaddam K, Bakht SM, Yang J, Jia W, Dell'Erba V, Assawes P, Shin SR, Dokmeci MR, Oklu R, Khademhosseini A, 3D Bioprinting for Tissue and Organ Fabrication, Ann. Biomed. Eng 45(1) (2017) 148–163. [PubMed: 27126775]

[17]. Blaeser A, Duarte Campos DF, Puster U, Richtering W, Stevens MM, Fischer H, Controlling Shear Stress in 3D Bioprinting is a Key Factor to Balance Printing Resolution and Stem Cell Integrity, Adv. Healthc. Mater 5(3) (2016) 326–333. [PubMed: 26626828]

[18]. Li H, Liu S, Li L, Rheological study on 3D printability of alginate hydrogel and effect of graphene oxide, Int. J. Bioprinting 2(2) (2016) 54–66.

[19]. Cui X, Dean D, Ruggeri ZM, Boland T, Cell damage evaluation of thermal inkjet printed chinese hamster ovary cells, Biotechnol. Bioeng. 106(6) (2010) 963–969. [PubMed: 20589673]

[20]. Gungor-Ozkerim PS, Inci I, Zhang YS, Khademhosseini A, Dokmeci MR, Bioinks for 3D bioprinting: an overview, Biomater. Sci 6(5) (2018) 915–946. [PubMed: 29492503]

[21]. Amer MH, Rose FR, Shakesheff KM, White LJ, A biomaterials approach to influence stem cell fate in injectable cell-based therapies, Stem cell Res. Ther 9(1) (2018) 39. [PubMed: 29467014]

[22]. Wan J, Microfluidic-based synthesis of hydrogel particles for cell microencapsulation and cell-based drug delivery, Polymers 4(2) (2012) 1084–1108.

[23]. Kang AR, Park JS, Ju J, Jeong GS, Lee SH, Cell encapsulation via microtechnologies, Biomaterials 35(9) (2014) 2651–2663. [PubMed: 24439405]

[24]. Rossow T, Lienemann PS, Mooney DJ, Cell Microencapsulation by Droplet Microfluidic Templating, Macromol. Chem. Phys 218(2) (2017) 1600380.

[25]. Bhatia SR, Khattak SF, Roberts SC, Polyelectrolytes for cell encapsulation, Curr. Opin. Colloid Interface Sci 10(1) (2005) 45–51.

[26]. Zhi ZL, Khan F, Pickup JC, Multilayer nanoencapsulation: A nanomedicine technology for diabetes research and management, Diabetes Res. Clin. Pract 100(2) (2013) 162–169. [PubMed: 23273839]

[27]. Granicka LH, Nanoencapsulation of cells within multilayer shells for biomedical applications. J. Nanosci. Nanotechnol 14(1) (2014) 705–716. [PubMed: 24730291]

[28]. Teramura Y, Iwata H, Bioartificial pancreas. Microencapsulation and conformal coating of islet of Langerhans, Adv. Drug Deliv. Rev 62(7) (2010) 827–840. [PubMed: 20138097]

[29]. Teramura Y, Kaneda Y, Iwata H, Islet-encapsulation in ultra-thin layer-by-layer membranes of poly(vinyl alcohol) anchored to poly(ethylene glycol)-lipids in the cell membrane, Biomaterials 28(32) (2007) 4818–4825. [PubMed: 17698188]

[30]. Velasco D, Tumarkin E, Kumacheva E, Microfluidic encapsulation of cells in polymer microgels, Small. 8(11) (2012) 1633–1642. [PubMed: 22467645]

[31]. Hong D, Park M, Yang SH, Lee J, Kim YG, Choi IS, Artificial spores: Cytoprotective nanoencapsulation of living cells, Trends Biotechnol. 31(8) (2013) 442–447. [PubMed: 23791238]

[32]. Park JH, Yang SH, Lee J, Ko EH, Hong D, Choi IS, Nanocoating of single cells: From maintenance of cell viability to manipulation of cellular activities, Adv. Mater 26(13) (2014) 2001–2010. [PubMed: 24452932]

[33]. Park JH, Hong D, Lee J, Choi IS, Cell-in-Shell Hybrids: Chemical Nanoencapsulation of Individual Cells, Acc. Chem. Res 49(5) (2016) 792–800. [PubMed: 27127837]

[34]. Yang SH, Hong D, Lee J, Ko EH, Choi IS, Artificial spores: Cytocompatible encapsulation of individual living cells within thin, tough Artificial shells, Small 9(2) (2013) 178–186. [PubMed: 23124994]

[35]. Kim BJ, Cho H, Park JH, Mano JF, Choi IS, Strategic Advances in Formation of Cell- in- Shell Structures: From Syntheses to Applications. Adv. Mater 30(14) (2018), 1706063.

[36]. Oliveira MB, Hatami J, Mano JF, Coating Strategies Using Layer-by-layer Deposition for Cell Encapsulation, Chem. - An Asian J 11(12) (2016) 1753–1764.

[37]. Serra M, Correia C, Malpique R, Brito C, Jensen J, Bjorquist P, Carrondo MJT, Alves PM, Microencapsulation technology: A powerful tool for integrating expansion and cryopreservation of human embryonic stem cells, PLoS One 6(8) (2011) e23212. [PubMed: 21850261]

[38]. Liu K, Deng Y, Zhang N, Li S, Ding H, Guo F, Liu W, Guo S, Zhao XZ, Generation of disk-like hydrogel beads for cell encapsulation and manipulation using a droplet-based microfluidic device, Microfluid. Nanofluidics 13(5) (2012) 761–767.

[39]. Kamperman T, Henke S, van den Berg A, Shin SR, Tamayol A, Khademhosseini A, Karperien M, Leijten J, Single Cell Microgel Based Modular Bioinks for Uncoupled Cellular Micro- and Macroenvironments, Adv. Healthc. Mater 6(3) (2017) 1600913.

[40]. Esfahani RR, Jun H, Rahmani S, Miller A, Lahann J, Microencapsulation of Live Cells in Synthetic Polymer Capsules, ACS Omega 2(6) (2017) 2839–2847. [PubMed: 30023677]

[41]. Lagus TP, Edd JF, A review of the theory, methods and recent applications of high-throughput single-cell droplet microfluidics, J. Phys. D. Appl. Phys 46(11) (2013) 114005.

[42]. Reece A, Xia B, Jiang Z, Noren B, McBride R, Oakey J, Microfluidic techniques for high throughput single cell analysis, Curr. Opin. Biotechnol 40 (2016) 90–96. [PubMed: 27032065]

[43E. Kemna WM, Schoeman RM, Wolbers F, Vermes I, Weitz DA, Van Den Berg A, High-yield cell ordering and deterministic cell-in-droplet encapsulation using Dean flow in a curved microchannel, Lab Chip 12(16) (2012) 2881–2887. [PubMed: 22688131]

[44]. Collins DJ, Neild A, deMello A, Liu AQ, Ai Y, The Poisson distribution and beyond: Methods for microfluidic droplet production and single cell encapsulation, Lab Chip 15(17) (2015) 3439–3459. [PubMed: 26226550]

[45]. Yang CG, Pan RY, Xu ZR, A single-cell encapsulation method based on a microfluidic multi-step droplet splitting system, Chinese Chem. Lett 26(12) (2015) 1450–1454.

[46]. Yin H, Marshall D, Microfluidics for single cell analysis, Curr. Opin. Biotechnol 23(1) (2012) 110–119. [PubMed: 22133547]

[47]. Wu L, Chen P, Dong Y, Feng X, Liu BF, Encapsulation of single cells on a microfluidic device integrating droplet generation with fluorescence-activated droplet sorting, Biomed. Microdevices 15(3) (2013) 553–560. [PubMed: 23404263]

[48]. Tan YC, Hettiarachchi K, Siu M, Pan YR, Lee AP, Controlled microfluidic encapsulation of cells, proteins, and microbeads in lipid vesicles, J. Am. Chem. Soc 128(17) (2006) 5656–5658. [PubMed: 16637631]

[49]. Aikawa T, Konno T, Ishihara K, Phospholipid polymer hydrogel microsphere modulates the cell cycle profile of encapsulated cells, Soft Matter. 9(18) (2013) 4628–4634.

[50]. Ma Y, Neubauer MP, Thiele J, Fery A, Huck WTS, Artificial microniches for probing mesenchymal stem cell fate in 3D, Biomater. Sci 2(11) (2014) 1661–1671.

[51]. Utech S, Prodanovic R, Mao AS, Ostafe R, Mooney DJ, Weitz DA, Microfluidic Generation of Monodisperse, Structurally Homogeneous Alginate Microgels for Cell Encapsulation and 3D Cell Culture, Adv. Healthc. Mater 4(11) (2015) 1628–1633. [PubMed: 26039892]

[52]. Hong J, Demello AJ, Jayasinghe SN, Bio-electrospraying and droplet-based microfluidics: Control of cell numbers within living residues, Biomed. Mater 5(2) (2010) 021001.

[53]. Tan WH, Takeuchi S, Monodisperse alginate hydrogel microbeads for cell encapsulation, Adv. Mater 19(18) (2007) 2696–2701.

[54]. Akbari S, Pirbodaghi T, Microfluidic encapsulation of cells in alginate particles via an improved internal gelation approach, Microfluid. Nanofluidics 16(4) (2014) 773–777.

[55]. Lee DH, Jang M, Park JK, Rapid one-step purification of single-cells encapsulated in alginate microcapsules from oil to aqueous phase using a hydrophobic filter paper: Implications for single-cell experiments, Biotechnol. J 9(10) (2014) 1233–1240. [PubMed: 25130499]

[56]. Mao AS, Shin JW, Utech S, Wang H, Uzun O, Li W, Cooper M, Hu Y, Zhang L, Weitz DA, Mooney DJ, Deterministic encapsulation of single cells in thin tunable microgels for niche modelling and therapeutic delivery, Nat. Mater 16(2) (2017) 236. [PubMed: 27798621]

[57]. Lienemann PS, Rossow T, Mao AS, Vallmajo-Martin Q, Ehrbar M, Mooney DJ, Single cell-laden protease-sensitive microniches for long-term culture in 3D, Lab Chip. 17(4) (2017) 727–737. [PubMed: 28154867]

[58]. Kamperman T, Henke S, Visser CW, Karperien M, Leijten J, Centering Single Cells in Microgels via Delayed Crosslinking Supports Long-Term 3D Culture by Preventing Cell Escape, Small 13(22) (2017) 1603711.

[59T. Yeung G.E. Gilbert, Shi J, Silvius J, Kapus A, Grinstein S, Membrane phosphatidylserine regulates surface charge and protein localization, Science 319 (2008) 210–213 [PubMed: 18187657]

[60]. Armstrong PB, On the role of metal cations in cellular adhesion: Effect on cell surface charge, J. Exp. Zool 163(1) (1966) 99–109. [PubMed: 5969747]

[61]. Kojima K, Maekawa A, Difference in electrokinetic charge of cells between two cell types of ascites hepatoma after removal of sialic acid, Cancer Res. 30(12) (1970) 2858–2862. [PubMed: 4321973]

[62]. Arnberg N, Kidd AH, Edlund K, Nilsson J, Pring-Åkerblom P, Wadell G, Adenovirus type 37 binds to cell surface sialic acid through a charge-dependent interaction, Virology 302(1) (2002) 33–43. [PubMed: 12429514]

[63]. Zhang Y, Yang M, Portney NG, Cui D, Budak G, Ozbay E, Ozkan M, Ozkan CS, Zeta potential: A surface electrical characteristic to probe the interaction of nanoparticles with normal and cancer human breast epithelial cells, Biomed. Microdevices 10(2) (2008) 321–328. [PubMed: 18165903]

[64]. V Bondar O, V Saifullina D, Shakhmaeva II, Mavlyutova II, Abdullin TI, Monitoring of the Zeta Potential of Human Cells upon Reduction in Their Viability and Interaction with Polymers, Acta Naturae. 4(1) (2012).

[65]. Krol S, Del Guerra S, Grupillo M, Diaspro A, Gliozzi A, Marchetti P, Multilayer nanoencapsulation. new approach for immune protection of human pancreatic islets, Nano Lett. 6(9) (2006) 1933–1939. [PubMed: 16968004]

[66]. Zhi ZL, Liu B, Jones PM, Pickup JC, Polysaccharide multilayer nanoencapsulation of insulin-producing β-cells grown as pseudoislets for potential cellular delivery of insulin, Biomacromolecules 11(3) (2010) 610–616. [PubMed: 20108955]

[67]. Ryan AJ, O'Neill HS, Duffy GP, O'Brien FJ, Advances in polymeric islet cell encapsulation technologies to limit the foreign body response and provide immunoisolation, Curr. Opin. Pharmacol 36 (2017) 66–71. [PubMed: 28865291]

[68]. Ai H, Fang M, Jones SA, Lvov YM, Electrostatic layer-by-layer nanoassembly on biological microtemplates: Platelets, Biomacromolecules 3(3) (2002) 560–564. [PubMed: 12005529]

[69]. Yu M, Ivanisevic A, Encapsulated cells: An atomic force microscopy study, Biomaterials 25(17) (2004) 3655–3662. [PubMed: 15020140]

[70]. Veerabadran NG, Goli PL, Stewart-Clark SS, Lvov YM, Mills DK, Nanoencapsulation of stem cells within polyelectrolyte multilayer shells, Macromol. Biosci 7(7) (2007) 877–882. [PubMed: 17599337]

[71]. Borkowska M, Godlewska E, Antosiak-Iwańska M, Kinasiewicz J, Strawski M, Szklarczyk M, Granicka LH, Suitability of polyelectrolyte shells modified with fullerene derivate for immunoisolation of cells. Experimental study, J. Biomed. Nanotechnol 8(6) (2012) 912–917. [PubMed: 23029999]

[72]. Choi D, Lee H, Kim HB, Yang M, Heo J, Won Y, Jang SS, Park JK, Son Y, Oh TI, Lee E, Hong J, Cytoprotective Self-assembled RGD Peptide Nanofilms for Surface Modification of Viable Mesenchymal Stem Cells, Chem. Mater 29(5) (2017) 2055–2065.

[73]. Fischer D, Li Y, Ahlemeyer B, Krieglstein J, Kissel T, In vitro cytotoxicity testing of polycations: influence of polymer structure on cell viability and hemolysis, Biomaterials 24(7) (2003) 1121–1131. [PubMed: 12527253]

[74]. Germain M, Balaguer P, Nicolas JC, Lopez F, Esteve JP, Sukhorukov GB, Winterhalter M, Richard-Foy H, Fournier D, Protection of mammalian cell used in biosensors by coating with a polyelectrolyte shell, Biosens. Bioelectron 21(8) (2006) 1566–1573. [PubMed: 16099641]

[75]. Kadowaki K, Matsusaki M, Akashi M, Control of cell surface and functions by layer-by-layer nanofilms, Langmuir 26(8) (2010) 5670–5678. [PubMed: 20055371]

[76]. Zhao Q, Li H, Li B, Nanoencapsulating living biological cells using electrostatic layer-by-layer selfassembly: Platelets as a model, J. Mater. Res 26(2) (2011) 347–351. [PubMed: 21359101]

[77]. Li W, Guan T, Zhang X, Wang Z, Wang M, Zhong W, Feng H, Xing M, Kong J, The effect of layer-by-layer assembly coating on the proliferation and differentiation of neural stem cells, ACS Appl. Mater. Interfaces 7(5) (2015) 3018–3029. [PubMed: 25347385]

[78]. Mansouri S, Fatisson J, Miao Z, Merhi Y, Winnik FM, Tabrizian M, Silencing red blood cell recognition toward anti-a antibody by means of polyelectrolyte layer-by-layer assembly in a twodimensional model system, Langmuir 25(24) (2009) 14071–14078. [PubMed: 19702281]

[79]. Mansouri S, Merhi Y, Winnik FM, Tabrizian M, Investigation of Layer-by-Layer Assembly of Polyelectrolytes on Fully Functional Human Red Blood Cells in Suspension for Attenuated Immune Response, Biomacromolecules 12(3) (2011) 585–592. [PubMed: 21306170]

[80]. Dzamukova MR, Zamaleeva AI, Ishmuchametova DG, Osin YN, Kiyasov AP, Nurgaliev DK, Ilinskaya ON, Fakhrullin RF, A direct technique for magnetic functionalization of living human cells, Langmuir 27(23) (2011) 14386–14393. [PubMed: 22032495]

[81]. Hamm CE, Merkel R, Springer O, Jurkojc P, Maiert C, Prechtelt K, Smetacek V, Architecture and material properties of diatom shells provide effective mechanical protection, Nature 421(69250 (2003) 841. [PubMed: 12594512]

[82]. Lee RBY, Mavridou DAI, Papadakos G, McClelland HLO, Rickaby REM, The uronic acid content of coccolith-associated polysaccharides provides insight into coccolithogenesis and past climate, Nat. Commun 7 (2016) 13144. [PubMed: 27782214]

[83]. Li C, Kaplan DL, Biomimetic composites via molecular scale self-assembly and biomineralization, Curr. Opin. Solid State Mater. Sci 7(4) (2003) 265–271.

[84]. Wang B, Liu P, Tang Y, Pan H, Xu X, Tang R, Guarding embryo development of zebrafish by shell engineering: A strategy to shield life from ozone depletion, PLoS One 5(4) (2010) e9963. [PubMed: 20376356]

[85]. Lee J, Choi J, Park JH, Kim MH, Hong D, Cho H, Yang SH, Choi IS, Cytoprotective silica coating of individual mammalian cells through bioinspired silicification, Angew. Chemie. Int. Ed 53(31) (2014) 8056–8059.

[86]. Yang SH, Ko EH, Choi IS, Cytocompatible encapsulation of individual Chlorella cells within titanium dioxide shells by a designed catalytic peptide, Langmuir. 28(4) (2012) 2151–2155. [PubMed: 22149097]

[87]. Matsusaki M, Kadowaki K, Nakahara Y, Akashi M, Fabrication of cellular multilayers with nanometer-sized extracellular matrix films, Angew. Chemie Int. Ed 119(25) (2007) 4773–4776.

[88]. Davidenko N, Schuster CF, Bax DV, Farndale RW, Hamaia S, Best SM, Cameron RE, Evaluation of cell binding to collagen and gelatin: a study of the effect of 2D and 3D architecture and surface chemistry, J. Mater. Sci. Mater. Med27(10) (2016) 148. [PubMed: 27582068]

[89A. Nishiguchi H Yoshida, M. Matsusaki, M. Akashi, Rapid construction of three-dimensional multilayered tissues with endothelial tube networks by the cell-accumulation technique, Adv. Mater 23(31) (2011) 3506–3510. [PubMed: 21728193]

[90]. Amano Y, Nishiguchi A, Matsusaki M, Iseoka H, Miyagawa S, Sawa Y, Seo M, Yamaguchi T, Akashi M, Development of vascularized iPSC derived 3D-cardiomyocyte tissues by filtration Layer-by-Layer technique and their application for pharmaceutical assays, Acta Biomater. 33 (2016) 110–121. [PubMed: 26821339]

[91]. Liu CY, Matsusaki M, Akashi M, The construction of cell-density controlled three-dimensional tissues by coating micrometer-sized collagen fiber matrices on single cell surfaces, RSC Adv. 4(86) (2014) 46141–46144.

[92]. Zheng W, Gao J, Song L, Chen C, Guan D, Wang Z, Li Z, Kong D, Yang Z, Surface-induced hydrogelation inhibits platelet aggregation, J. Am. Chem. Soc 135(1) (2013) 266–271. [PubMed: 23240879]

[93]. Lee J, Cho H, Choi J, Kim D, Hong D, Park JH, Yang SH, Choi IS, Chemical sporulation and germination: Cytoprotective nanocoating of individual mammalian cells with a degradable tannic acid-FeIII complex, Nanoscale 7(45) (2015) 18918–18922. [PubMed: 26528931]

[94]. Park T, Kim JY, Cho H, Moon HC, Kim BJ, Park JH, Hong D, Park J, Choi IS, Artificial spores: Immunoprotective nanocoating of red blood cells with supramolecular ferric ion-tannic acid complex, Polymers 9(4) (2017) 140.

[95]. Kim JY, Lee H, Park T, Park J, Kim MH, Cho H, Youn W, Kang SM, Choi IS, Artificial Spores: Cytocompatible Coating of Living Cells with Plant-Derived Pyrogallol, Chem. An Asian J 11(22) (2016) 3183–3187.

[96]. Abbina S, Siren EMJ, Moon H, Kizhakkedathu JN, Surface Engineering for Cell-Based Therapies: Techniques for Manipulating Mammalian Cell Surfaces, ACS Biomater. Sci. Eng (2017).

[97]. Yang J, Li J, Wang X, Li X, Kawazoe N, Chen G, Single mammalian cell encapsulation by in situ polymerization, J. Mater. Chem. B 4(47) (2016) 7662–7668.

[98]. Kim H, Shin K, Park OK, Choi D, Kim HD, Baik S, Lee SH, Kwon SH, Yarema KJ, Hong J, Hyeon T, Hwang NS, General and Facile Coating of Single Cells via Mild Reduction, J. Am. Chem. Soc 140(4) (2018) 1199–1202. [PubMed: 29281277]

[99]. Sakai S, Taya M, On-cell surface cross-linking of polymer molecules by horseradish peroxidase anchored to cell membrane for individual cell encapsulation in hydrogel sheath, ACS Macro Lett. 3(10) (2014) 972–975.

[100]. Sakai S, Nomura K, Mochizuki K, Taya M, Anchoring PEG-oleate to cell membranes stimulates reactive oxygen species production, Colloids Surfaces B Biointerfaces. 147 (2016) 336–342. [PubMed: 27544656]

[101]. Sakai S, Liu Y, Sengoku M, Taya M, Cell-selective encapsulation in hydrogel sheaths via biospecific identification and biochemical cross-linking, Biomaterials 53 (2015) 494–501. [PubMed: 25890746]

[102]. Takei T, Sugihara K, Ijima H, Kawakami K, In situ gellable sugar beet pectin via enzyme-catalyzed coupling reaction of feruloyl groups for biomedical applications, J. Biosci. Bioeng 112(5) (2011) 491–494. [PubMed: 21807557]

[103]. Partlow BP, Hanna CW, Rnjak-Kovacina J, Moreau JE, Applegate MB, Burke KA, Marelli B, Mitropoulos AN, Omenetto FG, Kaplan DL, Highly tunable elastomeric silk biomaterials, Adv. Funct. Mater 24(29) (2014) 4615–4624. [PubMed: 25395921]

[104]. Park KM, Ko KS, Joung YK, Shin H, Park KD, In situ cross-linkable gelatin-poly(ethylene glycol)-tyramine hydrogel via enzyme-mediated reaction for tissue regenerative medicine, J. Mater. Chem 21(35) (2011) 13180–13187.

[105]. Sinha RP, Häder D-P, UV-induced DNA damage and repair: a review, Photochem. Photobiol. Sci 1(4) (2002) 225–236. [PubMed: 12661961]

[106]. Eke G, Mangir N, Hasirci N, MacNeil S, Hasirci V, Development of a UV crosslinked biodegradable hydrogel containing adipose derived stem cells to promote vascularization for skin wounds and tissue engineering, Biomaterials 129 (2017) 188–198. [PubMed: 28343005]

[107]. Izadifar M, Chapman D, Babyn P, Chen X, Kelly ME, UV-assisted 3D bioprinting of nano-reinforced hybrid cardiac patch for myocardial tissue engineering, Tissue Eng. Part C Methods 24(2) (2017) 74–88. [PubMed: 29050528]

[108]. Liu VA, & Bhatia SN (2002). Three-dimensional photopatterning of hydrogels containing living cells. Biomedical microdevices, 4(4), 257–266.

[109]. Kantak C, Beyer S, Yobas L, Bansal T, Trau D, A ‘microfluidic pinball’for on-chip generation of Layer-by-Layer polyelectrolyte microcapsules, Lab Chip 11(6) (2011) 1030–1035. [PubMed: 21218225]

[110]. Shchukina EM, Shchukin DG, Layer-by-layer coated emulsion microparticles as storage and delivery tool, Curr. Opin. Colloid Interface Sci 17(5) (2012) 281–289.

Statement of Significance

The mechanical fragility of the plasma membrane and susceptibility to extracellular biochemical factors due to the lack of a physical barrier like a tough cell wall or exoskeleton make mammalian cells extra sensitive to harsh environmental conditions. This sensitively, in turn, limits the *ex vivo* storage, handling and manipulation of mammalian cells, as well as their *in vivo* applications. Environmental stresses such as exposure to UV, reactive chemicals and mechanical stress during biofabrication processes like 3D bioprinting can often compromise cell viability and function. Micro- and nanoencapsulation of single mammalian cells in protective shells have emerged as promising approaches to isolate cells from their surroundings and enhance resistance against perturbations in conditions during regenerative medicine and tissue engineering applications. In this review, the current state of art of single cell encapsulation strategies and the challenges associated with these technologies are discussed in detail. This is followed by the review of the protection provided by cell armor against a range of harsh *in vitro* and *in vivo* conditions.

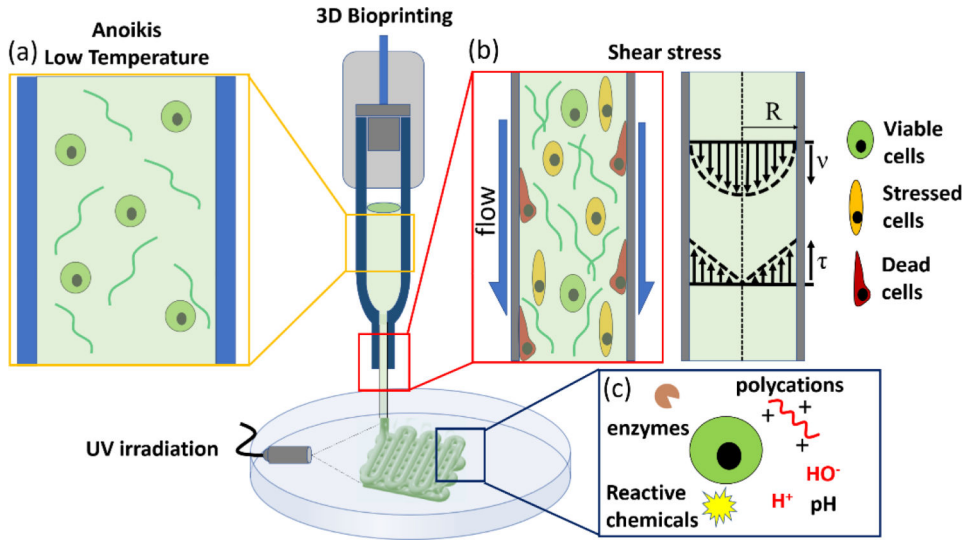

Figure 1.

Schematic illustration of the environmental stresses that cells are subjected during 3D bioprinting. (a) Cells suspended in the pre-hydrogel solution can be exposed to drops in temperature as well as anoikis due to lack of a matrix support in the syringe chamber. (b) Varying levels of shear stress is created in the printing nozzle depending on the pressure, solution viscosity and nozzle diameter. R, ν and τ represent nozzle radius, fluid velocity and shear stress distributions, respectively. (c) In the crosslinking solution after printing, cells should be able to survive various harsh conditions such as UV radiation, changes in pH and presence of reactive chemicals or enzymes depending on the crosslinking method employed.

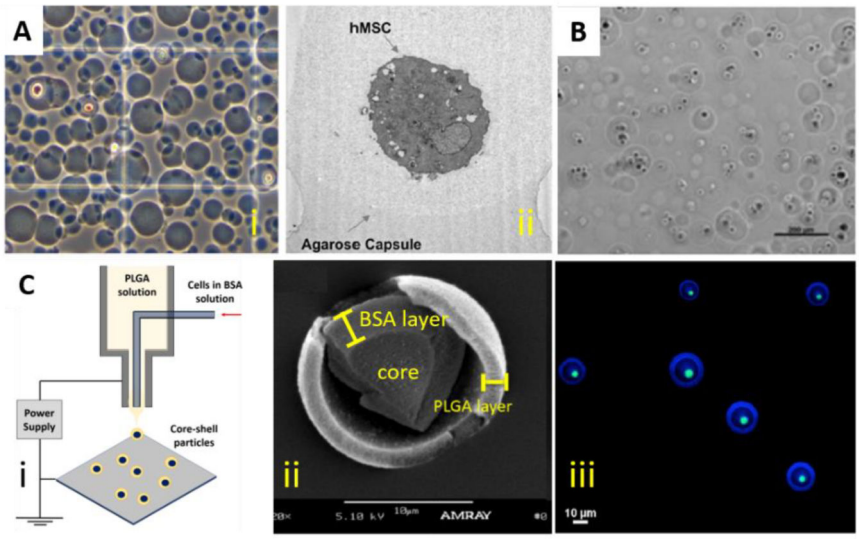

Figure 2.

Single cells encapsulated in micro-emulsified microgels or capsules. (A) (i) Phase contrast light (20X) and (ii) transmission electron microscopy images of hMSCs encapsulated on agarose microgels supplemented with fibronectin and fibrinogen. Reproduced with permission from ref 1. Copyright 2009 Elsevier Science. (B) Phase contrast microscopy image of hCSCs in agarose microbeads. Scale bar: 200 μm. Reproduced with permission from ref 2. Copyright 2014 Elsevier Science. (C) (i) Schematic illustration of the coaxial electrohydrodynamic jetting (EHD) of PLGA/BSA droplets with single cells forced through a coaxial needle under high electrical voltage. PLGA core-shell particles were obtained upon the evaporation of aqueous and organic solvents during the flight. (ii) SEM image of a cross-sectioned core-shell particle with outer PLGA and inner BSA layers. Scale bar: 10 μm. (iii) CLSM micrograph of GFP-NIH3T3 cells (green) encapsulated in the core of PLGA shell microparticles (blue). Reproduced with permission from ref 40. Copyright 2017 American Chemical Society.

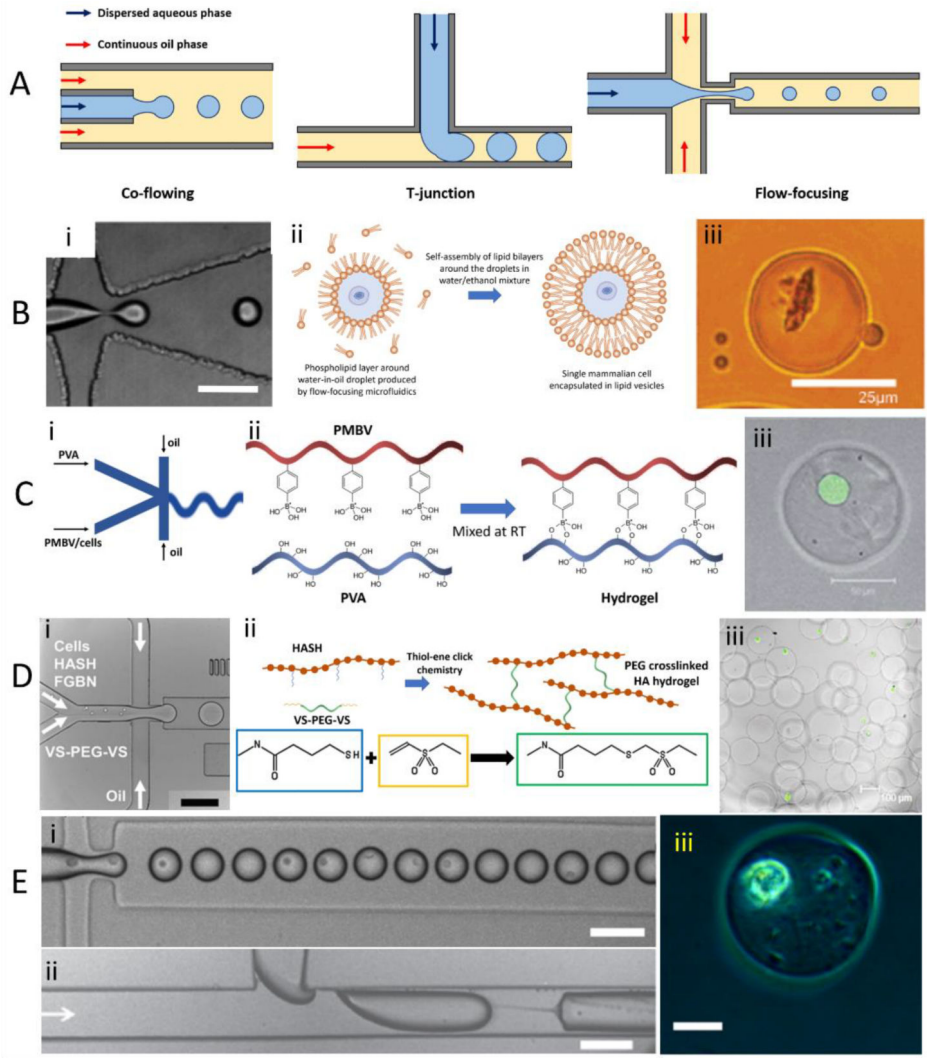

Figure 3.

Droplet-based microfluidics for the encapsulation of single cells. (A) Schematic representation of three main geometries of microfluidic designs to produce droplets periodically broken off from the flowing aqueous phase by the shear created by the continuous oil phase. Flow-focusing is the most widely employed approach for the microencapsulation of single cells. (B) Microencapsulation in lipid bilayers. (i) Production of lipid vesicles with aqueous cores using a flow focusing microfluidic device. Scale bar: 50 μm. (ii) Schematic illustration of the self-assembly of lipid bilayers around the aqueous droplets in water/ethanol mixture. (iii) Light microscopy image of single MCF-7 breast cancer cell encapsulated in DMPC vesicle. i and iii were reproduced with permission from ref 48. Copyright 2007 John Wiley and Sons. (C) Encapsulation in PMVB-PVA microgels. Schematic illustrations of (i) the flow-focusing design with separate inlets for PMBV/cell and PVA solutions and (ii) mechanism behind the reaction between the phenylboronic acid groups of PMBV and hydroxyl groups of PVA for hydrogelation. (iii) fluorescence microscopy image of a single HeLa cells encapsulated in PMBV-PVA hydrogel 8 h after encapsulation. Scale bar: 50μm. Reproduced with permission from ref 49. Copyright 2013

Taylor and Francis. (D) Encapsulation in PEG crosslinked HA microgels. (i) Bright field micrograph of the microfluidic setup used for the production of PEG crosslinked HA microgels. HASH and PEG-DV were injected through separate inlets to prevent premature gelation. Scale bar: 100 μm. (ii) Schematics of the crosslinking of HASH with PEG-DV. Thiol groups (SH) of HA react with the vinyl sulfone (VS) groups at the both ends of PEG via thio-ene click chemistry. (iii) Single viable hMSCs (green: calcein) encapsulated in HA-PEG microgels at 24 h of culture. i and iii were reproduced with permission from ref 50. Copyright 2014 Royal Society of Chemistry. (E) Production of alginate droplets encapsulating single cells using (i) T-junction and (ii) flow-focusing microfluidic devices. Formation of discrete droplets was hindered in T-junction device, therefore flow-focusing device was used for the encapsulation of single cells. Scale bars: 100 μm. (iii) Light microscopy image of a Jurkat T cell encapsulated in alginate microgel that was jetted into $CaCl_2$ bath for ionic crosslinking. Scale bar: 20 μm. Reproduced with permission from ref 52. Copyright 2010 Institute of Physics.

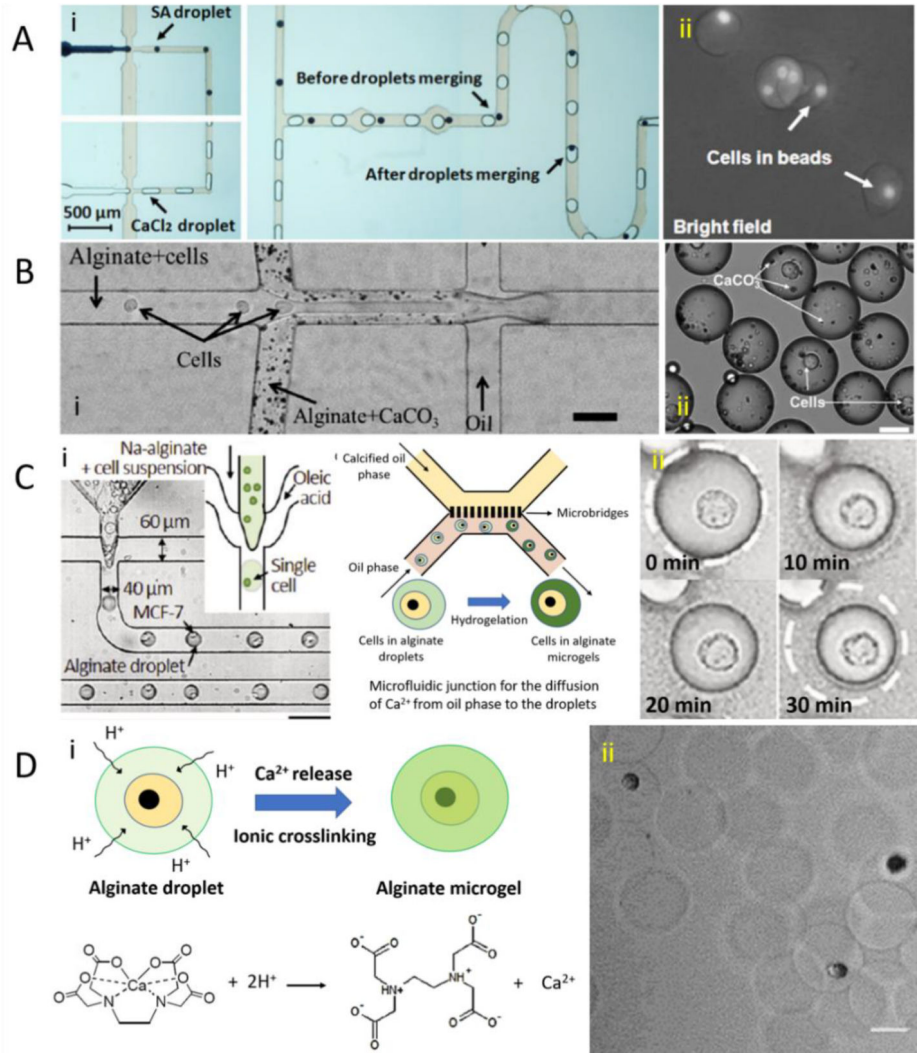

Figure 4.

Strategies utilized for the crosslinking of single cell encapsulating alginate droplets other than using a $CaCl_2$ bath. (A) Separate production and merging of alginate and calcium droplets. (i) Flow-focusing microfluidic setup with two parallel flow-focusing junctions for the separate production of alginate-cell and $CaCl_2$ droplets. Disc-shaped alginate microgels were obtained upon merging of the droplets in the serpentine channel. (ii) Bright field photograph of human HCT116 colon cancer cells immobilized in alginate microgels. Beads with more than single cell were also observed. Reproduced with permission from ref 38. Copyright 2012 American Chemical Society. (B) Use of water insoluble $CaCO_3$ particles in the alginate droplets. (i) Bright-field image of the microfluidic setup with two flow-focusing junctions in series to produce single cell encapsulating alginate microgels. $CaCO_3$ particles were mixed with the cell suspension at the first junction to prevent potentially cytotoxic early nanoparticle-cell interactions. Droplets were formed at the second junction. Scale bar: 50 µm. (ii) Bright field image of the droplets with M6C cells and $CaCO_3$ nanoparticles before crosslinking of alginate. Alginate was crosslinked upon solubilization of $CaCO_3$ with acetic acid that diffused from the oil phase into the droplets. Scale bar: 25 µm. Reproduced

with permission from ref 54. Copyright 2014 American Chemical Society. (C) Use of a second calcified oil phase. (i) Bright field micrograph of the flow-focusing device with the schematics of a second junction for the introduction of calcified oil phase. Scale bar: 50 μm. Calcium ions diffused from the oil phase into the droplets triggered crosslinking of alginate droplets. Microbridges prevented the escape of droplets into the calcified oil stream. (ii) Bright field micrographs of alginate microbeads encapsulating MCF-7 cells in oil suspension at different time points. The volume of the beads was found to decrease over time due to evaporation of water. i and iii were reproduced with permission from ref 55. Copyright 2014 John Wiley and Sons. (D) Use of Ca-EDTA complex in the droplets. (i) Schematics explaining the alginate crosslinking upon acidification of the droplets and subsequent release of calcium ions from EDTA. (ii) Bright field micrograph of alginate microgels with single hMSCs. Majority of the microbeads were found to be empty due to Poisson distribution. Scale bar: 25 μm. Reproduced with permission from ref 51. Copyright 2015 John Wiley and Sons.

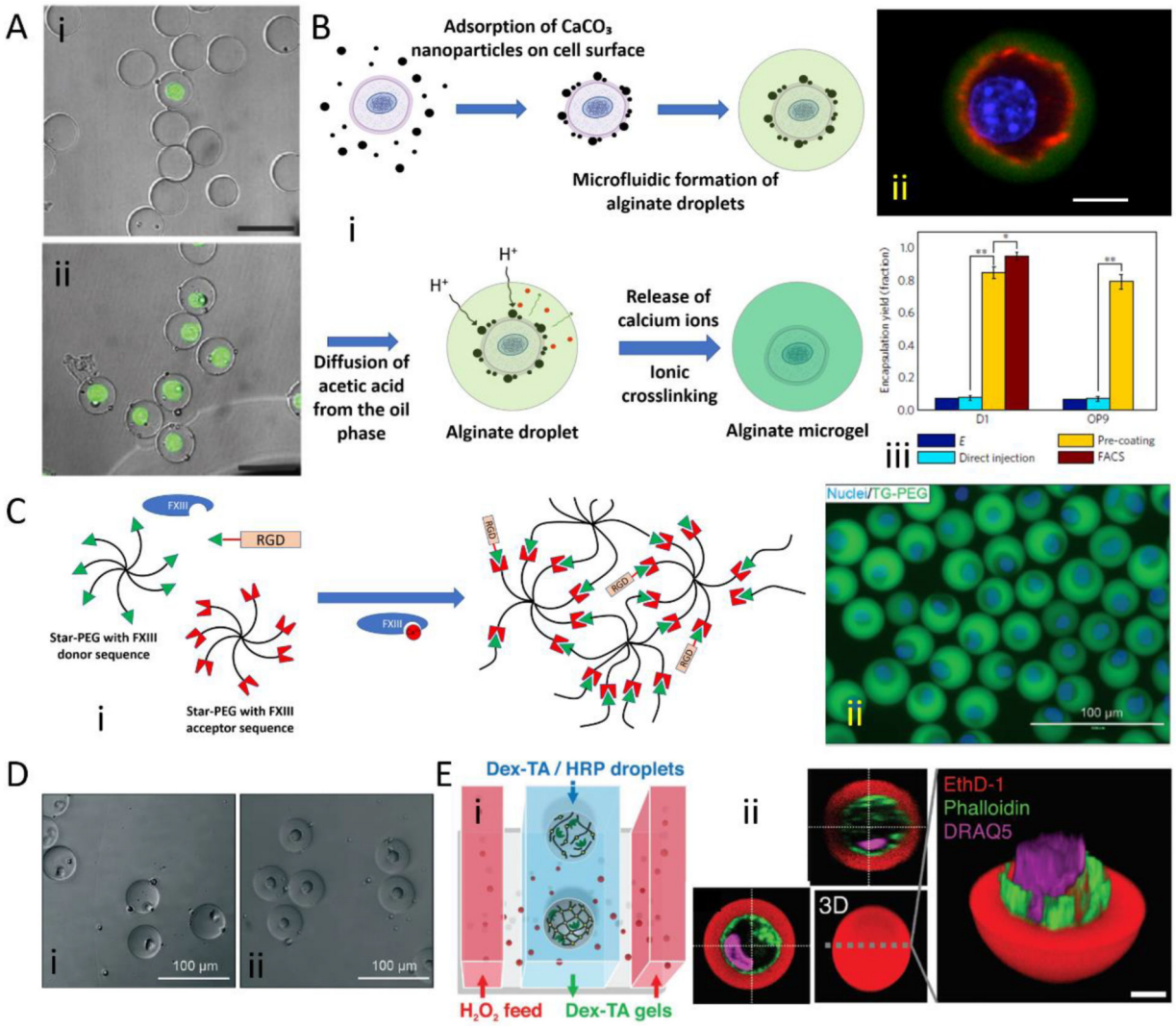

Figure 5.

Strategies reported to improve single cell encapsulation yield (A-C) and to prevent off-center immobilization of cells (D-E) in the microgels. (A) FACS sorting. Fluorescent micrographs of UV crosslinked PEGDA microgels (i) before and (ii) after FACS sorting based on the presence of single viable bovine chondrocytes (green:calcein) showed that the yield of microgels with single cells increased from 10% to over 90%. Scale bars: 50 μm. Reproduced with permission from ref 39. Copyright 2017 John Wiley and Sons. (B) $CaCO_3$ adsorption on the cells for ionic crosslinking of alginate droplets. (i) Schematic illustration of pre-coating the cells with $CaCO_3$ nanoparticles. Release of calcium ions from the $CaCO_3$ nanoparticles upon reaction with acetic acid allowed alginate only in cell-laden droplets to gel. (ii) Confocal micrograph of single mMSC immobilized in an alginate microgel. (green: alginate, blue: nucleus, red: actin cytoskeleton). Scale bar: 10 μm. (iii) Yield of encapsulation of CaCO3 pre-coated mMSC and OP9 cells compared to direct encapsulation and FACS sorting. ii and iii were reproduced with permission from ref 56. Copyright 2017 Nature Publishing Group. (C) $CaCO_3$ adsorption on the cells for the FXIII mediated hydrogel crosslinking. (i) Schematic illustration of the covalent crosslinking of star-PEG

hydrogels by calcium-activated enzyme FXIII. RGD peptides were included in the reaction to introduce cell-adhesive sequences in the microgels. Release of calcium ions from the $CaCO_3$ adsorbed on the cells allowed activation of FXIII and crosslinking of star-PEG only in cell-laden droplets. (ii) Fluorescence micrographs of single hMSC-laden FITC-labeled star-PEG microgels. (green: alginate, blue: cell nucleus). Reproduced with permission from ref 57. Copyright 2017 Royal Society of Chemistry. (D) Phase contrast images of cell-laden star-PEG microgels (i) before and (ii) after shaking on an orbital shaker. All cells were repositioned in the center of the droplets after shaking. Reproduced with permission from ref 57. Copyright 2017 Royal Society of Chemistry. (E) Cell repositioning in the microgels by delayed crosslinking. (i) Schematic illustration of the 3-channel microfluidic devices showing the gradual diffusion of H_2O_2 through the PDMS walls into the cell-laden droplets for the delayed crosslinking of tyramine modified dextran molecules by HRP. (ii) Confocal micrographs of a Dex-TRA microgel confirming the repositioning of single hMSC in the center of the microgel. Scale bar: 5 μm. Reproduced with permission from ref 58. Copyright 2017 John Wiley and Sons.

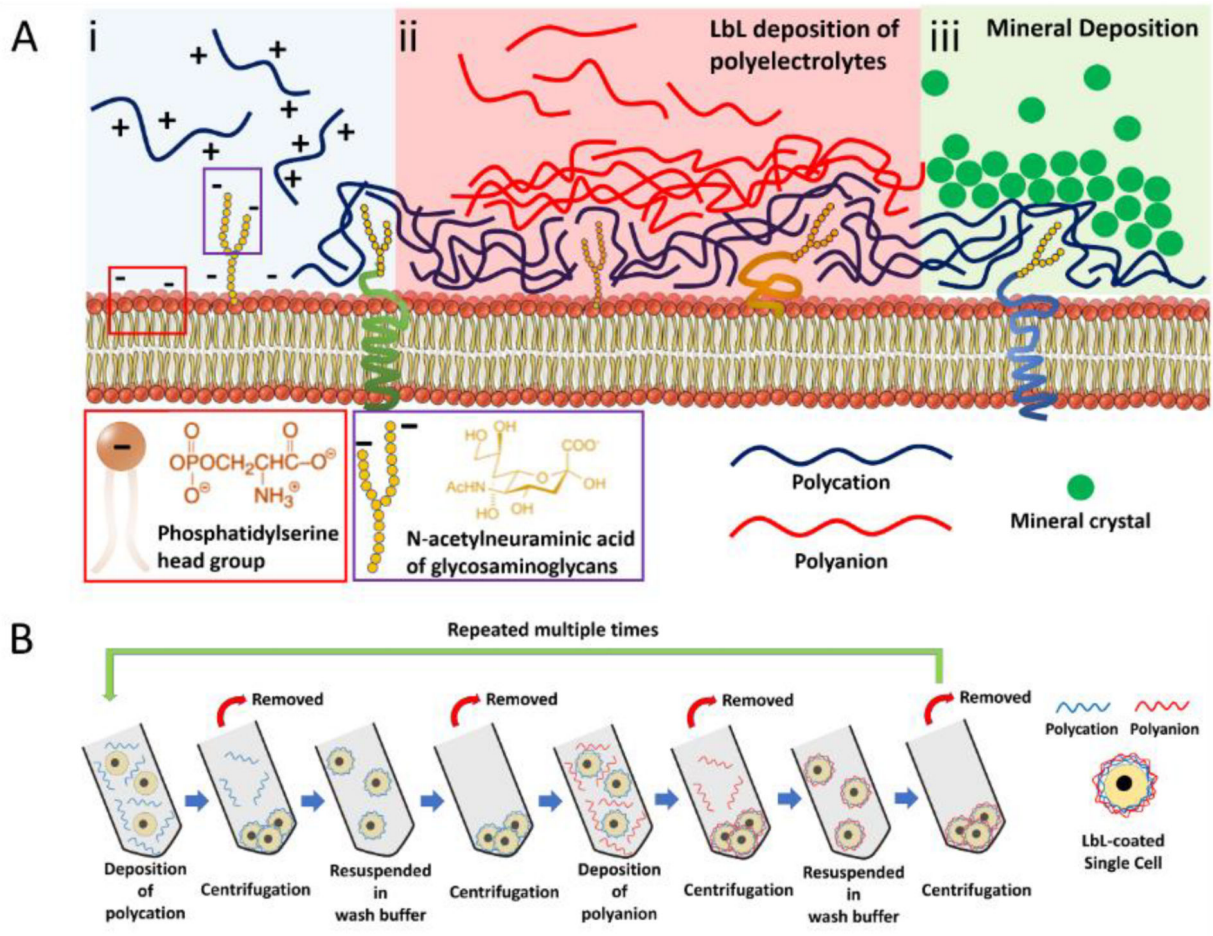

Figure 6.

Electrostatic deposition of nanofilms on the cells. (A) Schematic illustration of the mechanism behind nanocoating by electrostatic interactions. (i) Phospholipids with negatively charged head groups such as phosphatidylserine and the sialic acid moieties of membrane glycosaminoglycans provide a net negative charge to the surface of mammalian cells, allowing for the deposition of positively charged molecules on the plasma membrane. (ii) Incubation of polycation-coated cells in polyanion solution leads to alternation of the surface charge, which allows for the LbL deposition of polyelectrolyte layers on the cells. (iii) Minerals such as silica and titania can also be deposited on the polyelectrolyte pre-coated cells through electrostatic interactions. (B) LbL nanocoating of cells by centrifugation as the most widely employed approach for electrostatic deposition of polyelectrolytes. After the deposition of each layer, cells are collected by centrifugation, washed with buffer and then collected again by centrifugation.

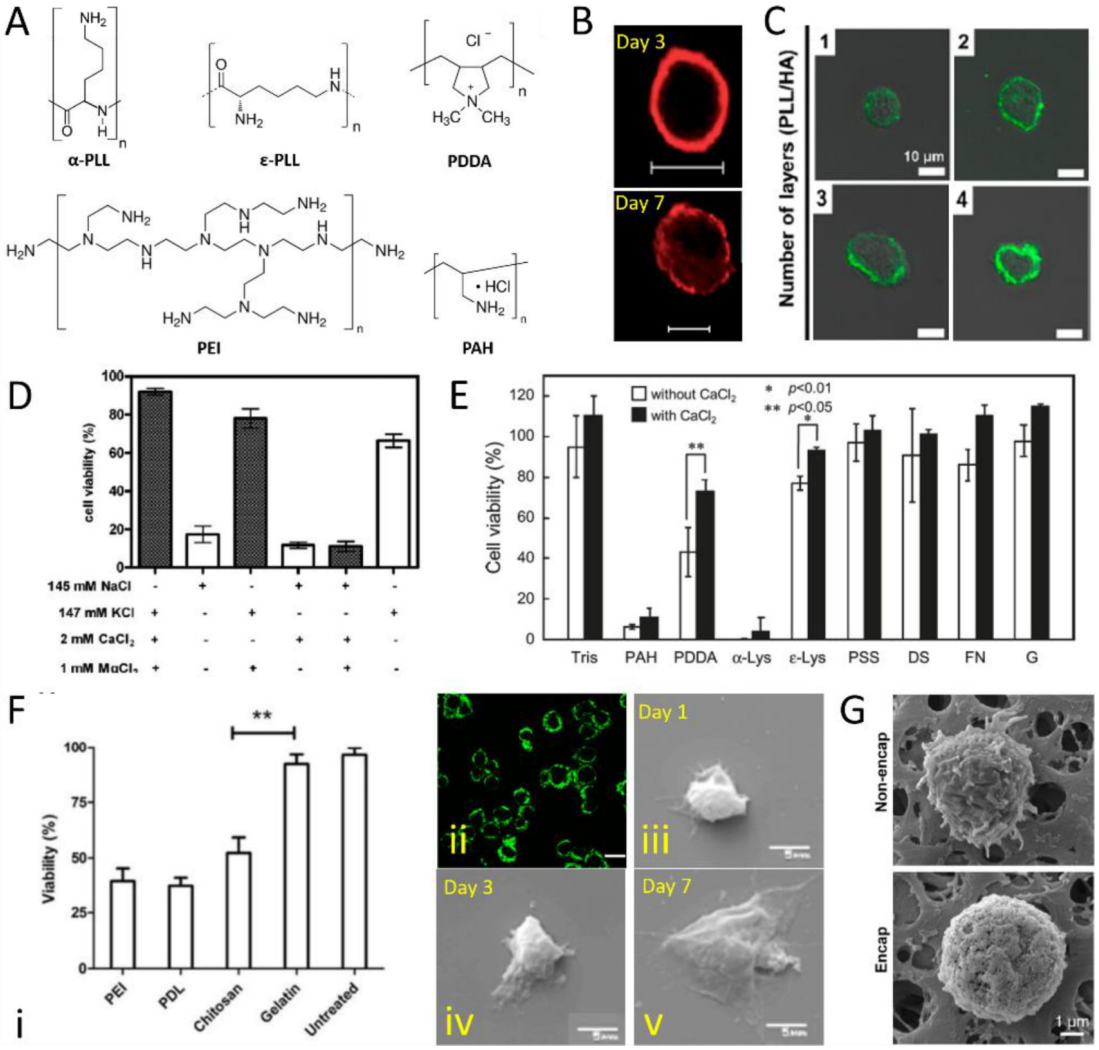

Figure 7.

Nanocoating of single mammalian cells with polyelectrolytes. (A) Common synthetic polycations used for deposition on negatively charged mammalian cells. (B) Confocal images of mMSCs nanocoated with 6 bilayers of PLL/HA at 3 and 7 days after encapsulation. Diffusion of the discrete fluorescent layer observed on day 3 into the cell on day 7 indicated internalization of the FITC-PLL by the cells. Reproduced with permission from ref 70. Copyright 2007 John Wiley and Sons. (C) Confocal images of mMSCs nanocoated with different number of PLL-FITC and HA-FITC layers. Fluorescent intensity on the cells was found to increase with increasing number of layers deposited. Reproduced with permission from ref 72. Copyright 2017 American Chemical Society. (D) Viability of MELN cells coated with 4 bilayers of PDDA/PSS in buffers with different compositions. Presence of potassium ions in the coating buffer was found to improve cell viability while sodium, calcium or magnesium ions did not. Reproduced with permission from ref 74. Copyright 2006 Elsevier Science. (E) Viability of L929 murine fibroblasts incubated in various polyelectrolytes and proteins. α-PLL was found to be highly toxic while ε-PLL with lower molecular weight performed significantly better. Calcium ions in the incubation buffer

slightly reduced the toxicity of polyelectrolytes. DS: dextran sulfate, G: gelatin. Reproduced with permission from ref 75. Copyright 2010 American Chemical Society. (F) LbL nanoencapsulation of hNSCs. (i) Viability of hNSCs coated with various synthetic and natural polycations. Gelatin (type A) was chosen for LbL nanocoating because of its significantly lower toxicity compared to synthetic PEI or natural chitosan. (ii) Confocal micrographs of hNSCs LbL coated with FITC-GL/AL bilayers. A discrete fluorescent layer was observed around the cells. Scale bar: 10 μm. (ii-v) SEM micrographs of a nanocoated hNSC on days 1, 3 and 7. Cells unable to spread on day 1 were found to start spreading at later time points, indicating the degradation of nanofilm encapsulating the cells. Reproduced with permission from ref 77. Copyright 2015 American Chemical Society. (G) SEM micrographs of native and nanoencapsulated Jurkat T cells. A clear change in the cell surface topography was observed upon deposition of CH/AL bilayers. Reproduced with permission from ref 5. Copyright 2016 American Chemical Society.

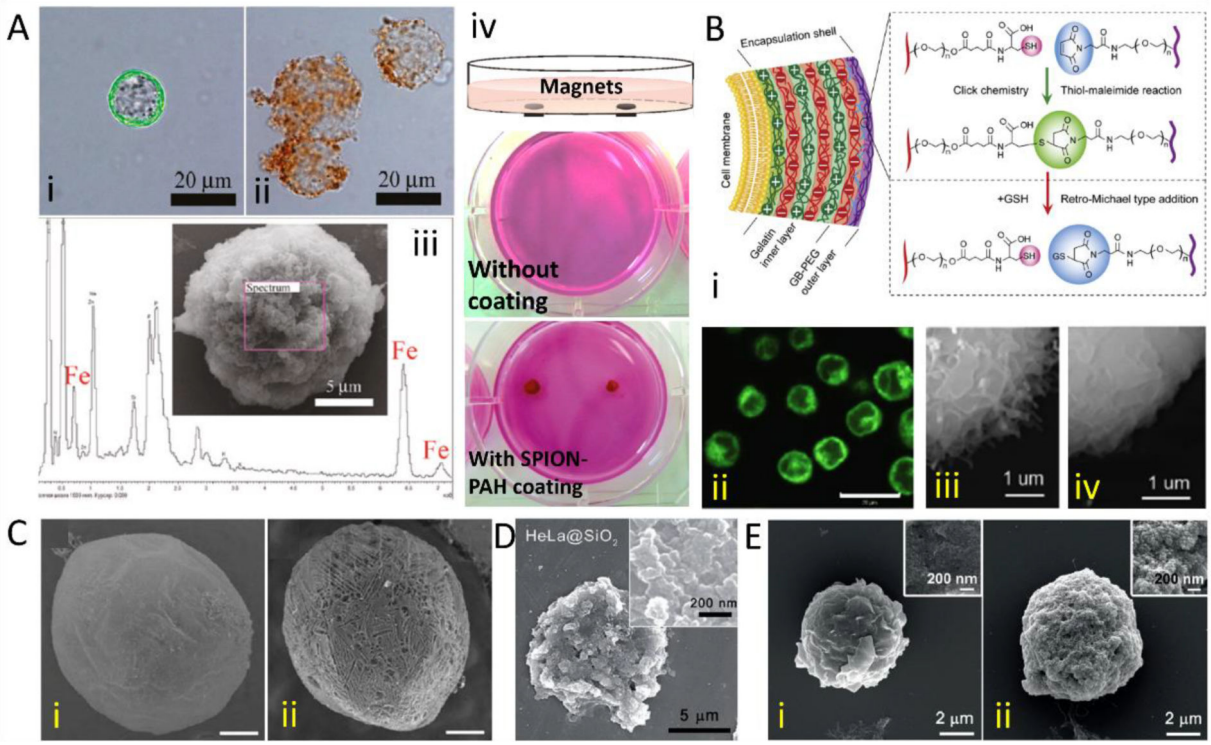

Figure 8.

Electrostatic deposition of modified polyelectrolytes (A-B) and minerals (C-D). (A) Deposition of magnetic SPION-conjugated PAH on HeLa cells. Fluorescence micrographs of HeLa cells coated with (i) FITC-PAH and (ii) SPION-PAH. The characteristic brown color of SPION indicated deposition of magnetic particles on the cells. (iii) EDX spectrum of the nanolayer formed on the HeLa cells confirmed the deposition of Fe-based SPIONs. (iv) Photographs of native and SPION-PAH coated HeLa cells suspended in a petri dish with two circular magnets positioned on the bottom. SPION-PAH coated cells were shown to align on the magnets, confirming the functionalization of the cells. Reproduced with permission from ref 80. Copyright 2011 American Chemical Society. (B) Nanocoating of HeLa cells with gelatin inner and crosslinked PEG outer layers. (i) Schematic illustration of the reaction mechanism of PEG crosslinking on the gelatin bilayers by thiol-maleimide click chemistry and degradation. (ii) Confocal micrographs of HeLa cells nanocoated with 5 bilayers of GL-A/GL-B (green: FITC- GL-B). Scale bar: 20 μm. SEM micrographs of (iii) uncoated and (iv) nanocoated HeLa cells. Note the change in surface topography after nanofilm deposition. Reproduced with permission from ref 11. Copyright 2017 Elsevier Science. (C) SEM micrographs of (i) bare and (ii) lanthanide phosphate nanocoated zebrafish eggs. Surfaces of the eggs were primed with CH/PAA prior to mineral deposition. A crystalline morphology was obtained after nanocoating. Scale bars: 200 μm. Reproduced with permission from ref 84. Copyright 2010 Public Library of Science. (D) SEM micrograph of a HeLa cells nanoencapsulated in a silica shell. Cell surface was primed with PEI before the deposition of negatively charged silica particles. Reproduced with permission from ref 85. Copyright 2014 John Wiley and Sons. (E) SEM micrographs of Jurkat T cells (i) before and (ii) after encapsulation in titania nanoshell. Cell membrane was primed with

PEI before the nucleation of titania on cell surface. Reproduced with permission from ref 10. Copyright 2017 John Wiley and Sons.

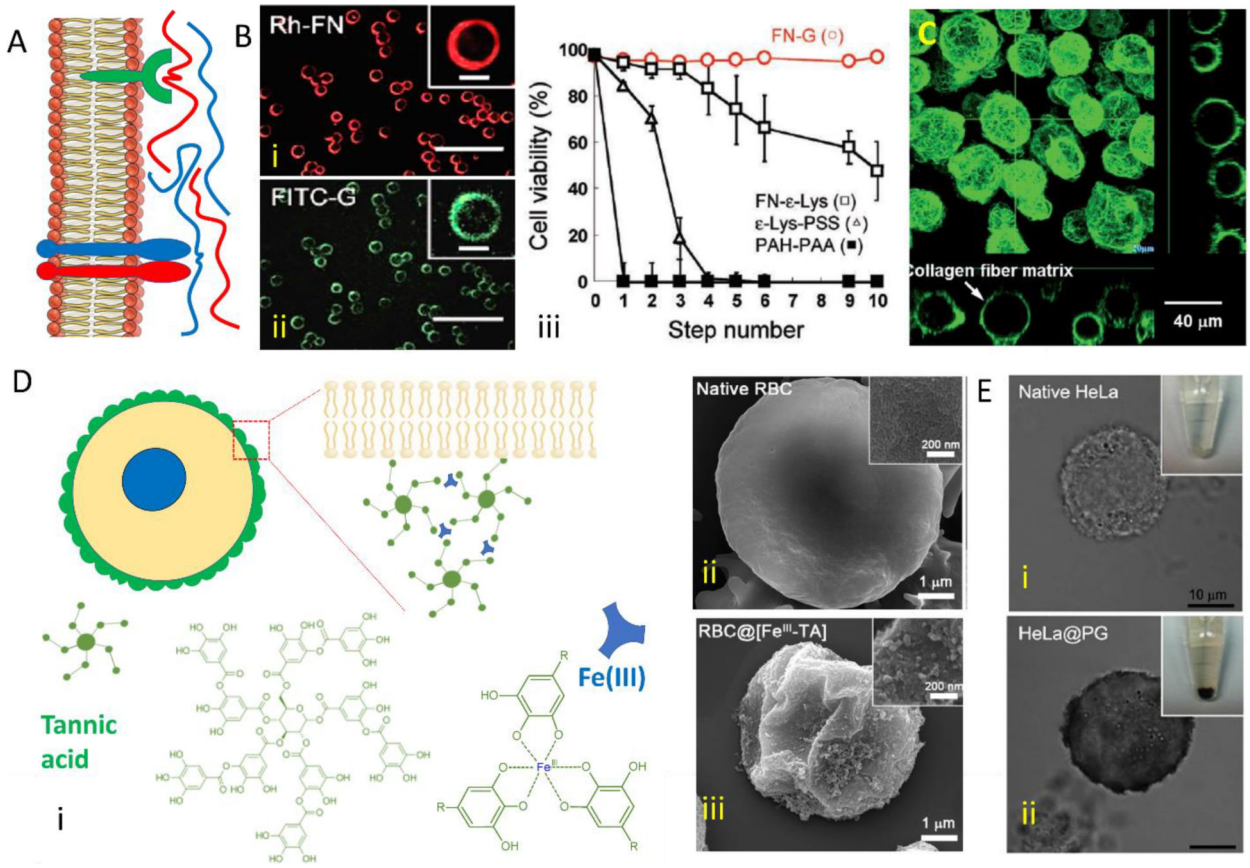

Figure 9.

Deposition of nanolayers by (A-C) receptor-ligand and (D-F) non-specific interactions. (A) Schematic illustration of the deposition of nanolayers by receptor-ligand interactions. Integrin-RGD tripeptide and CD44-HA have been the most common interactions exploited for single cell nanocoating with ECM-derived macromolecules. (B) (i) Rhodamine B-FN and (ii) FITC-GL layers shown in the fluorescent micrographs of L929 murine fibroblasts nanocoated with 9 layers of FN/GL. Scale bars: 10 μm. (iii) Viability of L929 fibroblasts at each step of deposition with various ECM protein and polyelectrolyte couples. Deposition of FN/GL by receptor-ligand interactions was found to be significantly less cytotoxic than the deposition of polyelectrolytes. Reproduced with permission from ref 89. Copyright 2011 John Wiley and Sons. (C) Confocal micrograph of human dermal fibroblasts coated with self-assembling FITC labeled Col-I triple helices. Reproduced with permission from ref 91. Copyright 2014 Royal Society of Chemistry. (D) Deposition of TA-Fe(III) metal-organic complex nanolayers on the cells. (i) Schematic representation of the deposition of plant-derived TA on cell surface via nonspecific interactions and formation of a nanolayer of metal-organic complex via crosslinking with Fe(III) ions. (ii) SEM micrographs of (ii) native and (iii) Ta-Fe(III) nanocoated hRBCs. A distinct morphological change can be observed in nanoencapsulated cell. ii and iii were reproduced with permission from ref 94. Copyright 2017 Elsevier Science. (E) Phase contrast micrograph of HeLa cells (i) before and (ii) after nanocoating with PG. Auto-oligomerization of PG on surfaces allowed for formation of

nanolayers on the cells. Reproduced with permission from ref 95. Copyright 2016 John Wiley and Sons.

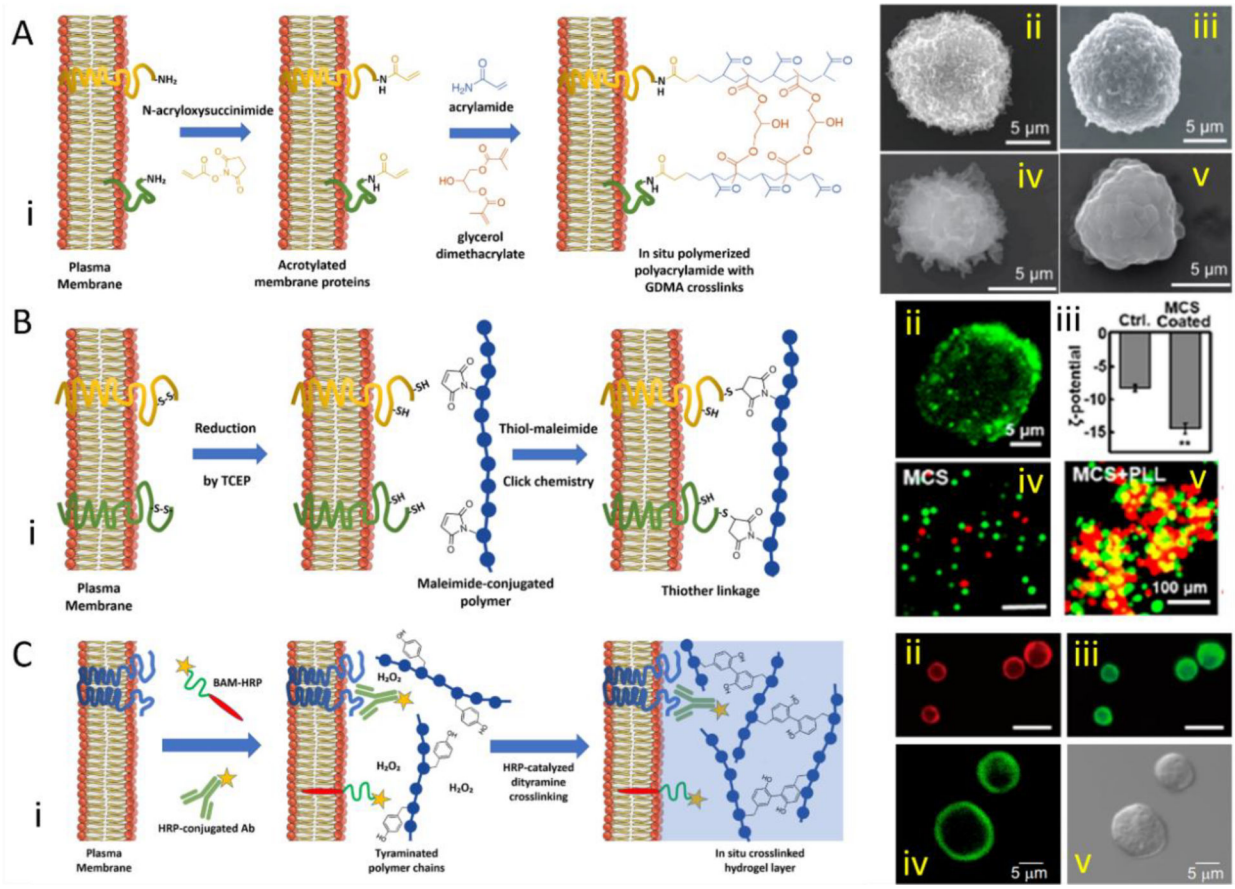

Figure 10.

Nanolayer deposition by membrane modification. (A) *In situ* polymerization of hydrogels on plasma membrane. (i) Schematic representation of the nanocoating with polyacrylamide polymerized on the acrotylated N-termini of membrane proteins and crosslinked with glycerol dimethacrylate. SEM micrographs of the native and polyacrylamide nanocoated (ii, iv) hMSCs and (iii, v) BACs, respectively. Surface of the cells became smoother upon nanoencapsulation in polyacrylamide hydrogels. Reproduced with permission from ref 97. Copyright 2016 Royal Society of Chemistry. (B) Deposition of polymer nanolayers by covalent attachment to membrane proteins. (i) Schematic representation of the deposition of polymer nanolayers via the covalent bonds formed between the thiol groups of reduced membrane proteins and maleimide groups of the polymer chains. (ii) Confocal micrograph of reduced HeLa cells coated with maleimide-conjugated CS-FITC. (iii) Comparison of the zeta potentials of native and CS nanocoated HeLa cells. CS coating increased the negative charge of the cell surface, resulting in (iv) repulsion between individual cells and allowing for (v) bridging of coated cells with PLL. (green: cells stained with DiO, red: cells stained with DiI). Reproduced with permission from ref 35. Copyright 2018 John Wiley and Sons. (C) In situ crosslinking of hydrogels on cell surface. (i) Schematic illustration of in situ crosslinking polymer chains with tyramine groups via dityramine reaction catalyzed by HRP in the presence of hydrogen peroxide. HRP was immobilized on cell membrane either by HRP-conjugated antibodies specific to cell surface proteins or HRP-conjugated BAM inserted into plasma membrane. (ii) Ph-GL and (iii) Ph-PVA layers shown in the confocal

micrographs of HeLa cells nanoencapsulated in GL-PVA hydrogel nanolayers. Cells were treated with BAM-HRP for immobilization of HRP on cell surface. Scale bars: 40 μm. Reproduced with permission from ref 99. Copyright 2014 American Chemical Society. (iv) Confocal and (v) phase contrast micrographs of HepG2 cells nanoencapsulated in FITC labeled Ph-AL hydrogel nanolayers. CD326 positive HepG2 cells were selectively labeled with HRP-conjugated anti-CD326 antibodies for the immobilization of HRP on the cell membrane. Reproduced with permission from ref 101. Copyright 2015 Elsevier Science.

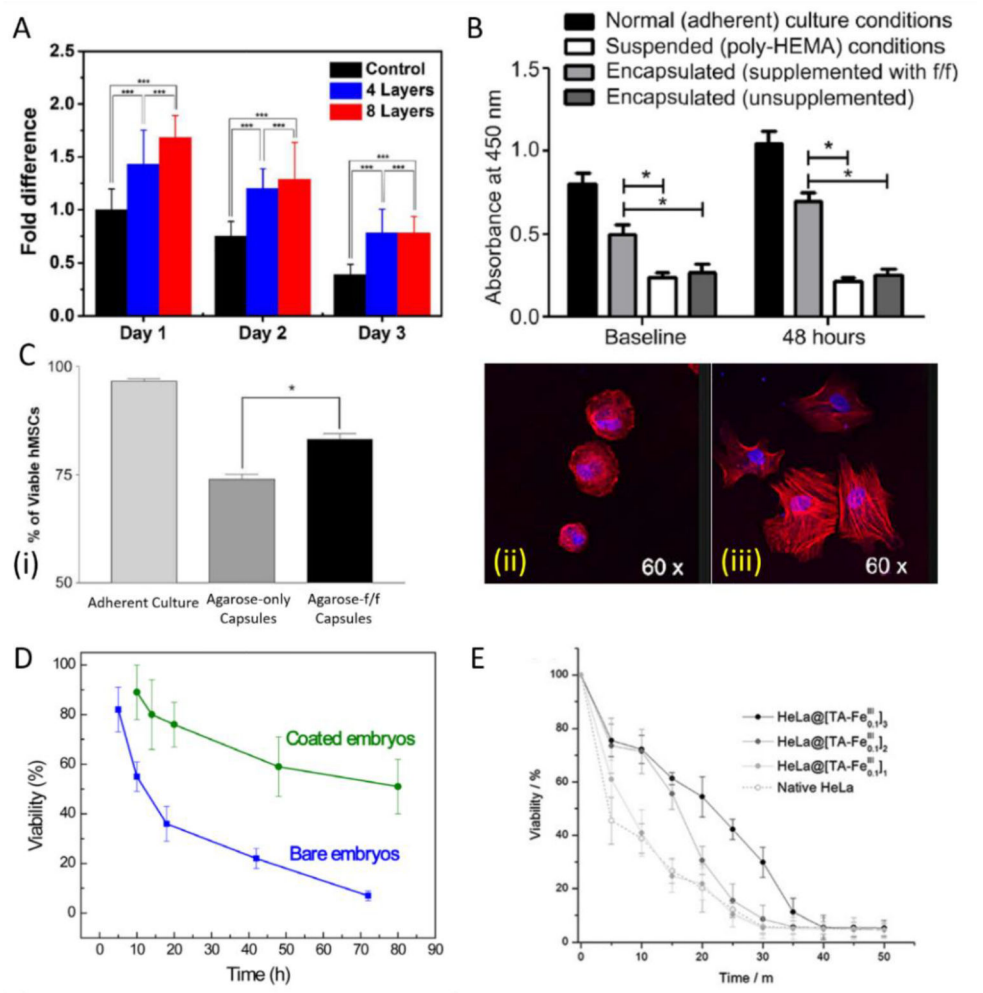

Figure 11.

Protection of encapsulated single mammalian cells from (A-C) anoikis and (D-E) UV irradiation. (A) Normalized proportions of the metabolic activities of hMSCs nanocoated with 2 or 4 bilayers of Col/HA compared to uncoated cells after 3 days of culture on poly-HEMA coated surface. Metabolic activities were determined by MTT assay. Nanocoating with ECM components provided a clear protection against anoikis. Reproduced with permission from ref 3. Copyright 2017 American Chemical Society. (B) Relative metabolic activities of hCSCs encapsulated in agarose microgels with or without fibrinogen/fibronectin (f/f) supplementation after baseline (16 h) and 48 h culture on poly-HEMA coated surfaces compared to native cells suspended on poly-HEMA and adherent on tissue culture plastic. Metabolic activities were quantified using CCK-8 assay. Agarose-(f/f) microgels was found to improve cell viability significantly over 2 days of culture in an attachment-deprived state. Reproduced with permission from ref 2. Copyright 2014 Elsevier Science. (C) Similar findings were reported also for hMSCs. (i) Viabilities of hMSCs encapsulated in agarose microgels with and without fibrinogen/fibronectin (f/f) supplementation and cultured on non-adhesive poly-HEMA surfaces for 24 h compared to the native cells cultured on tissue culture plastic. Survival rate of native cells cultured on poly-HEMA surface was around 70%. Fluorescent micrographs of the encapsulated cells showed that (ii) the cells in agarose-

only microgels had a spherical morphology with little cytoskeletal organization while the cells in agarose-(f/f) microgels displayed spreading and organization of actin cytoskeleton. (red: actin filaments, blue: nucleus). Reproduced with permission from ref 1. Copyright 2009 Elsevier Science. (D) Viabilities of the bare and $LnPO_4$ coated zebrafish eggs under UV-B radiation over 80 h of exposure. UV absorption by the mineral coat provided long-term protection against irradiation. Reproduced with permission from ref 84. Copyright 2010 Public Library of Science. (E) Viabilities of native and TA-Fe(III) coated HeLa cells under short-term UV-C radiation. The metal-organic complex nanocoat provided protection against UV radiation, which increased with increasing numbers of layers deposited. Reproduced with permission from ref 93. Copyright 2015 Royal Society of Chemistry.

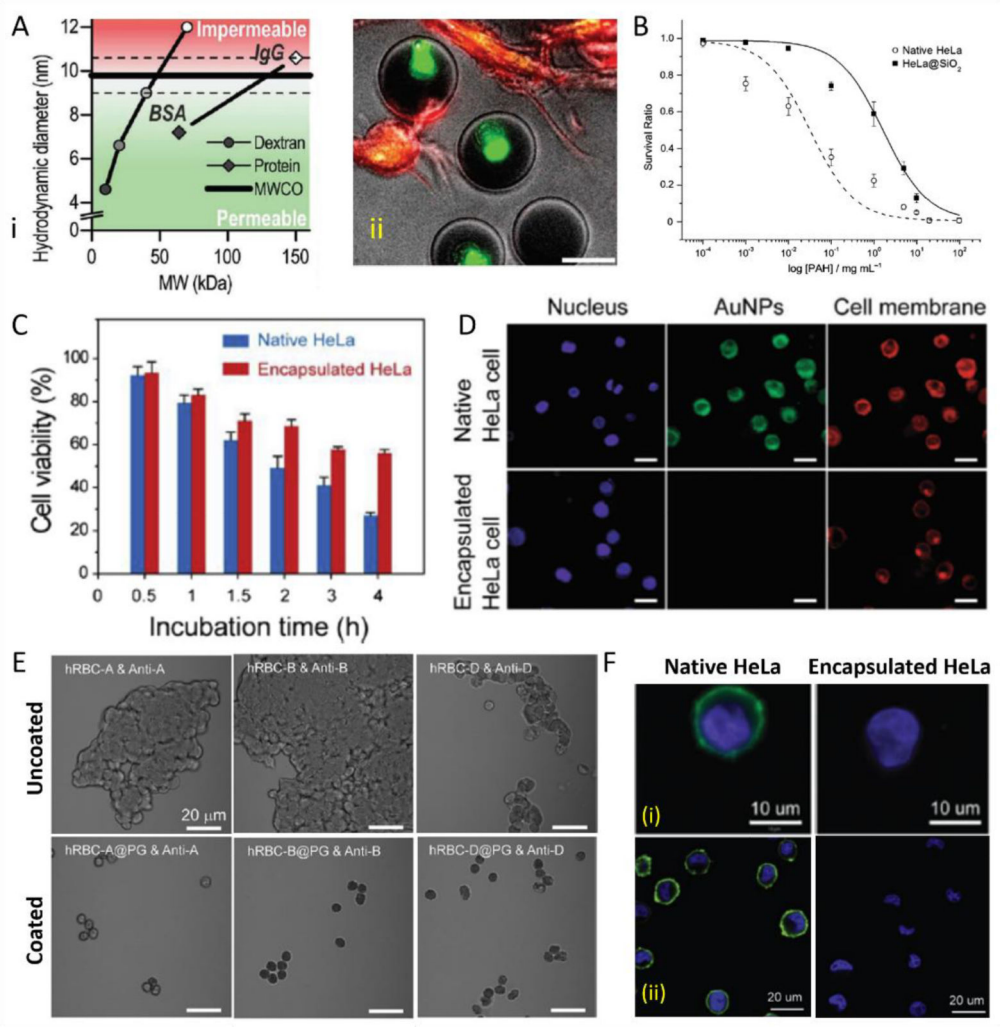

Figure 12.

Protection of single mammalian cells against cytotoxic large macromolecules by encapsulating shells with size-selective permeability. (A) Size-selective permeability of UV-crosslinked PEGDA microgels. (i) Permeability of microgels against dextran of various molecular weights, BSA and IgG antibody. Microgels allowed for the diffusion of BSA (66 kDa) and dextran of 50 kDa and less, while it blocked IgG of 150 kDa. It was found to be impermeable to molecules with a hydrodynamic diameter higher than 10 nm (ii) Confocal micrograph of hMSCs encapsulated in PEGDA microgels cocultured with human endothelial cells in fibrin macrogels. hMSCs were isolated from their microenvironment: endothelial cells could not penetrate the microgels. Reproduced with permission from ref 39. Copyright 2017 John Wiley and Sons. (B) Survival ratios of the native and silica coated HeLa cells incubated in PAH solutions of a series of concentrations. PAH concentration required for coated cells was almost 10 fold higher than that required for uncoated cells to reduce survival ratio to 0.2, indicating a barrier effect of silica nanocoat against polycations. Reproduced with permission from ref 85. Copyright 2014 John Wiley and Sons. (C) Viabilities of native and coated HeLa cells over 4 h incubation in 0.1% (w/v) trypsin-EDTA solution. GL/PEG nanolayers restricted the accessibility of trypsin to cell membrane,

limiting its proteolytic activity on the membrane proteins. Reproduced with permission from ref 11. Copyright 2017 Elsevier Science. (D) Confocal micrographs of the native and polyacrylamide nanocoated HeLa cells incubated in FITC-labeled PEG-coated gold nanoparticles. Lack of FITC signal in the coated cells indicated that hydrogel sheaths on the cells prevented the internalization of gold nanoparticles with a diameter of 80 nm by blocking its interactions with the cell membrane. Reproduced with permission from ref 97. Copyright 2016 Royal Society of Chemistry. (E) Phase contrast images of naked and PG coated hRBCs incubated with their anti-type antibodies. Uncoated cells agglutinated and formed large clusters while coated cells behaved like 0-type RBCs, suggesting that the PG nanolayers masked the surface antigens and inhibited the binding of anti-type antibodies. Reproduced with permission from ref 95. Copyright 2016 John Wiley and Sons. (F) Confocal micrographs of native and coated HeLa cells showed that (i) polyacrylamide (Reproduced with permission from ref 97. Copyright 2016 Royal Society of Chemistry) and (ii) GL-PEG nanolayers (Reproduced with permission from ref 11. Copyright 2017 Elsevier Science) prevented the binding of FITC-labeled anti-CD44 antibodies to CD44 antigens on cell surface (blue: nucleus).

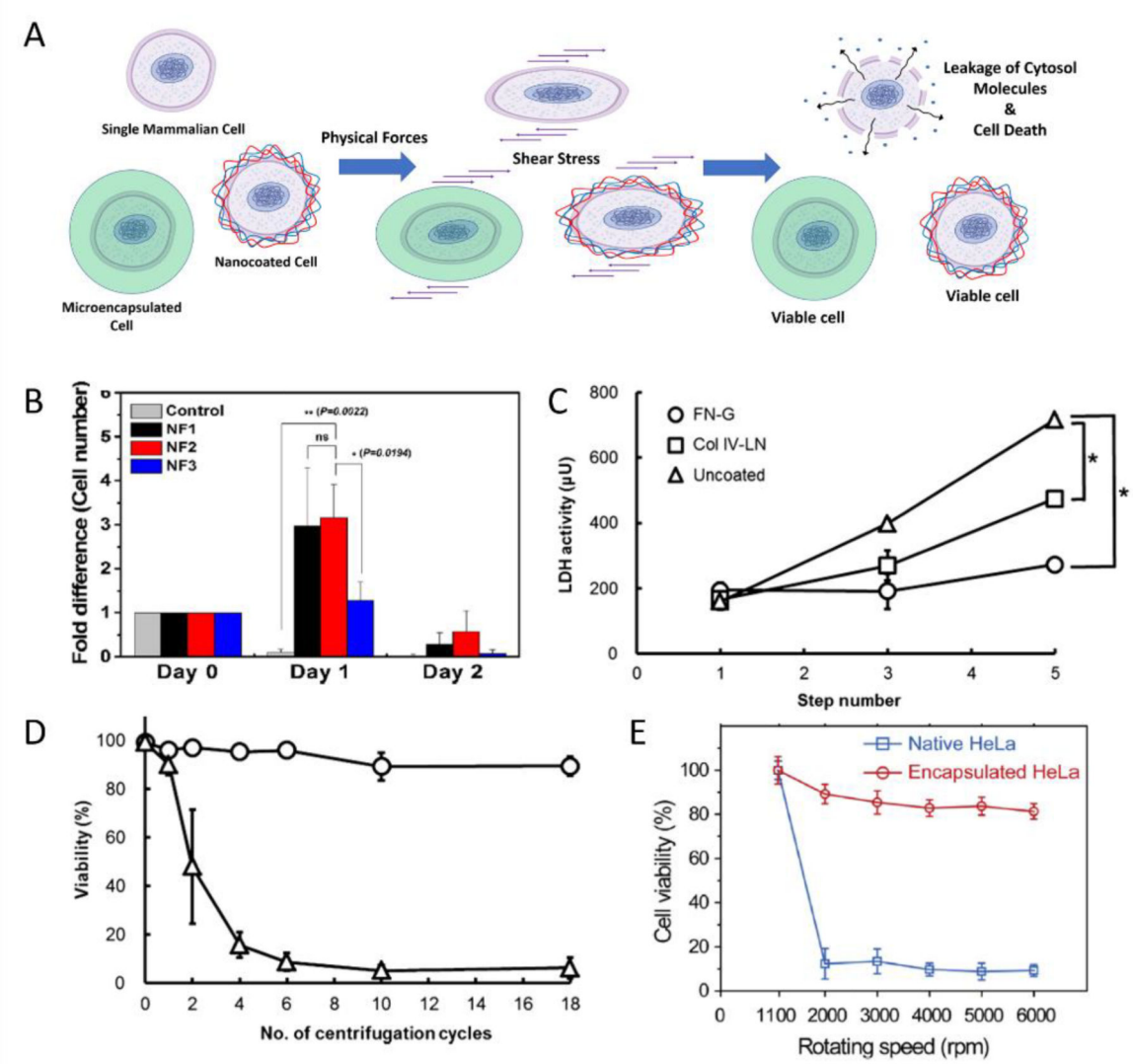

Figure 13.

Protection of encapsulated cells from mechanical stress. (A) Schematic illustration of the shielding effect of micro- and nanoshells against physical forces. Protective shells prevent the shear stress-induced damaging of plasma membrane and therefore the leakage of cytosol molecules, preserving the integrity and viability of single cells. (B) Comparison of the number of viable MSCs with or without nanocoating cultured under continuous agitation. Nanocoats significantly improved the cell viability during 24 h of continuous mechanical stress. NF1: $(PLL/RGD)_3$, NF2: $(PLL/HA)/(PLL/RGD)_2$, NF3: $(PLLA/HA)_3$. Reproduced with permission from ref 72. Copyright 2017 American Chemical Society. (C) Activity of LDH leaked from HepG2 cells exposed to several cycles of centrifugal forces. FN/GL and Col-IV/LN nanocoats significantly reduced LDH activity, indicating less membrane damage and leakage of cytosol molecules compared to naked cells (D) Comparison of the viabilities of naked and FN/GL coated HepG2 cells during 18 cycles of centrifugation. Significantly higher survival of coated cells indicated effective protection by the nanocoats against mechanical stress. Reproduced with permission from ref 9. Copyright 2012 American

Chemical Society. (E) Viabilities of naked and GL-PEG coated HeLa cells that were centrifuged 6 times at various centrifugal speeds. Nanocoated cells were able to survive even the extremes of speeds while viability of the naked cells dramatically dropped even at slightly faster speeds. Reproduced with permission from ref 11, Copyright 2011 Elsevier Science.

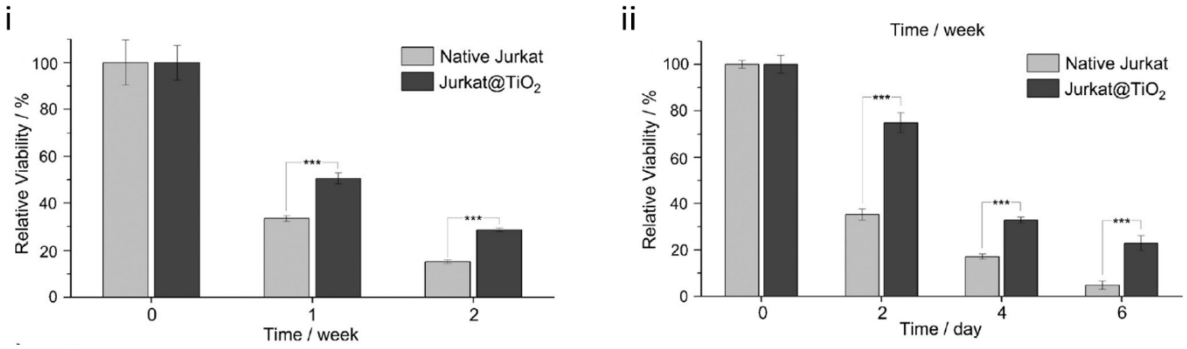

Figure 14.

Protection of single cells against non-culture temperatures by nanoencapsulation. Higher viabilities of nanocoated Jurkat T cells than uncoated counterparts after long-term incubation at (i) 25°C and (ii) 40°C indicated improved survival of the cells at non-culture conditions *in vitro.* Reproduced with permission from ref 10. Copyright 2017 John Wiley and Sons.

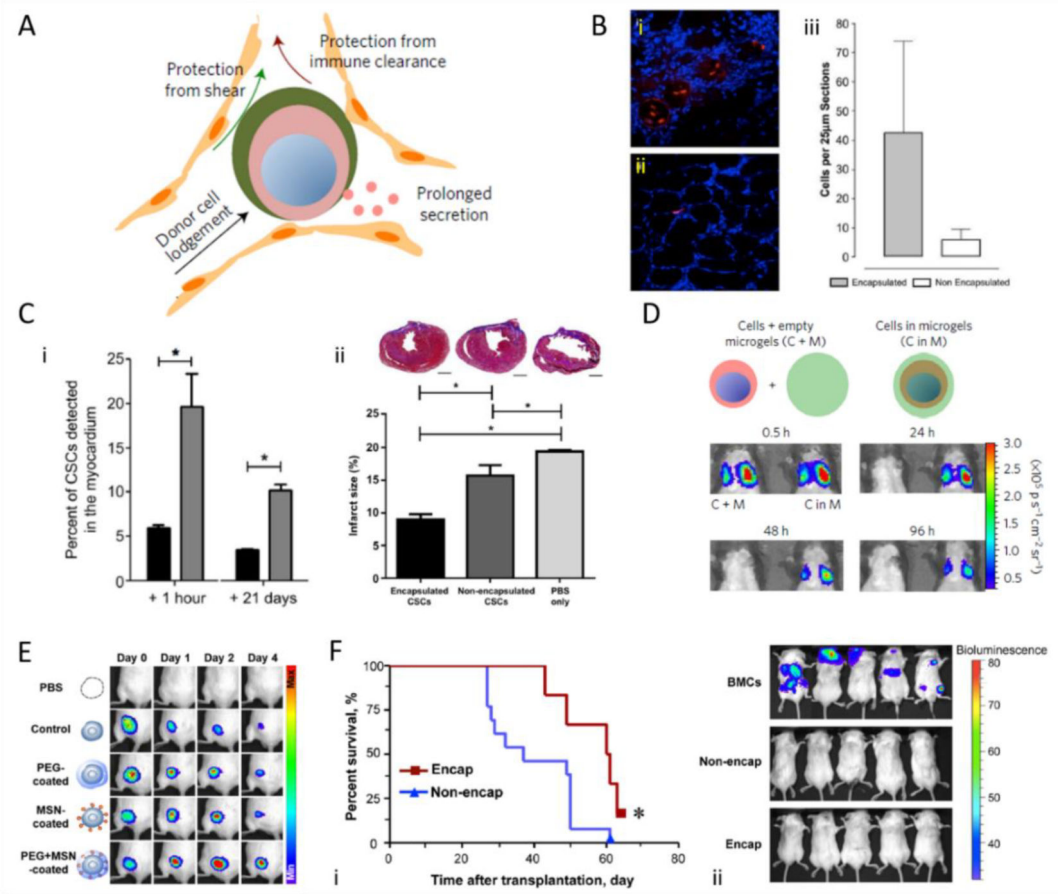

Figure 15.

In vivo performance of encapsulated single mammalian cells. (A) Schematic illustration of the protection provided by cell encapsulation against in vivo stresses including shear stress in the veins and immune clearance by the host. Reproduced with permission from ref 56. Copyright 2017 Nature Publishing Group. (B*) In vivo* retention of hMSCs injected to hindlimbs of Fisher 344 rats. Confocal micrographs of (i) agarose-(f/f) microencapsulated and (ii) bare cells 3 days after injection. (Red: hMSCs, blue: counterstain) (iii) Comparison of the number of cells with and without microcapsules in the sections of gastrocnemius muscle. Microencapsulation enhanced the retention of xenotransplanted hMSCs significantly. Reproduced with permission from ref 1. Copyright 2009 Elsevier Science. (C) In vivo performance of hCSCs in a myocardial infarction model. (i) Comparison of the percent of cells with or without agarose-(f/f) retained in the myocardium. Black bar: non-encapsulated, grey bar: microencapsulated. (ii) Comparison of the infarct sizes at 3 weeks post-transplantation between encapsulated, non-encapsulated and blank groups. Findings suggested improved retention and therapeutic activity provided by microencapsulation of single hCSC cells. Reproduced with permission from ref 2. Copyright 2014 Elsevier Science. (D) Bioluminescence graphs of F. luciferase-expressing mMSCs transplanted into the lungs of mice with or within alginate microgels. Naked cells injected with empty microgels were found to be cleared completely only 24 h after transplantation while the microencapsulated cells were retained even after 4 days. Reproduced with permission from

ref 56. Copyright 2017 Nature Publishing Group. (E) Luminescence images showing the biodistribution of luciferase-expressing HeLa cells with or without PEG or MSN coating, or both. Dual nanolayers of MSNs and PEG hydrogels on the cell surface increased the duration of *in vivo* retention in mice with normal immunity, suggesting that PEG coating with dexamethasone release from the MSNs helped the cells escape the immune system of the host up to a certain degree over 4 days of observation. Reproduced with permission from ref 35. Copyright 2018 John Wiley and Sons. (F) Protection of immune deficient host against hostility of allogeneic immune cells. (i) Survival ratios of the BALB/c mice transplanted with naked and CH/AL nanocoated mouse T cells. The viability of mice injected with uncoated cells started decreasing dramatically 30 days after injection due to grafts versus host disease (GVHD), while over 60% of the hosts injected with coated cells were alive at day 60. (ii) Bioluminescence imaging of immune-deficient mice injected with BMCs. Unlike the control group that were injected with only BMCs, mice transplanted with both BMCs and naked or nanocoated T cells showed no evidence of tumor formation over 70 days of observation, meaning that nanocoating did not impair the anti-tumor activity T cells. Reproduced with permission from ref 5. Copyright 2016 American Chemical Society.

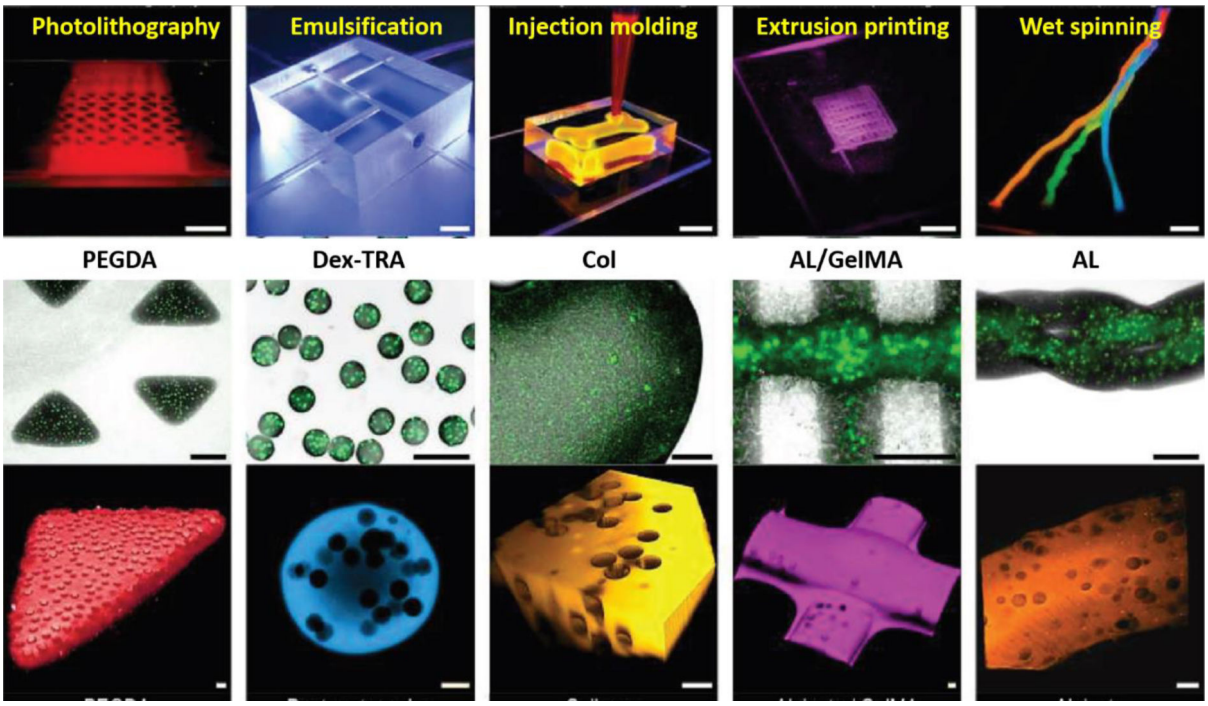

Figure 16.

Incorporation of encapsulated single mammalian cells into 3D biofabrication practices. Leijten and co-workers employed various biofabrication methods (top row, scale bars: 5000 μm) and bioink materials (middle row, scale bars: 500 μm) mixed with FACS sorted single hMSCs-laden PEGDA microgels to fabricate a variety of 3D constructs (bottom row, scale bars: 50 μm). In the confocal micrographs of the constructs, single-cell laden microgels were observed to be distributed homogenously throughout the macrogels. Reproduced with permission from ref 39. Copyright 2017 John Wiley and Sons.

Table 1.

Strategies for the microencapsulation of single mammalian cells.

Materials used	Strategy	Solidification/Crosslinking method	Advantages	Disadvantages	Cell types encapsulated
Agarose with fibrinogen/ fibronectin	Microemulsification in oil by vortexing	Thermal gelation (temperature drop)	Mild encapsulation conditions, high cell viability	Polydispersity of microgels and low single cell encapsulation efficiency	hMSCs [1] hCSCs [2]
PLGA	Coaxial electrohydrodynamic jetting (EHD) of coreshell particles	Evaporation of organic and aqueous solvents during the flight of the particles	Small core size allowing for encapsulation of only single cells	Reduced cell viability due to EHD	NIH3T3 fibroblasts [40]
DOPC/DMPC/ DPPC	flow-focusing microfluidics	Self-assembly of phospholipid polar heads around the aqueous droplets followed by the formation of lipid bilayers in water/ethanol mixture	High cell viability after encapsulation	Large capsule size increasing the chance of encapsulation of multiple cells	HeLa cells CF-7 breast cancer cells [48]
PMBV – PVA	flow-focusing microfluidics	Crosslinking by reaction between the phenylboronic acid and hydroxyl groups	Radical-free reaction allows for high cell viability, tunable hydrogel stiffness	Low $_{efficiency}$ single cell encapsulation	HeLa cells [49]
HASH – PEG-DVS	flow-focusing microfluidics	Crosslinking by click chemistry reaction between thiol and vinyl sulfone groups	Radical-free reaction allows for high cell viability, tunable hydrogel stiffness	Lack of cell spreading leading to spherical morphology and tendency towards adipogenic differentiation	hMSCs [50]
Alginate	flow-focusing microfluidics	Bioelectrospraying (BES) of the droplets into $CaCl_2$ bath	High cell viability and proliferation rates	Decrease in final concentration of alginate in the droplets	Jurkat T cells[52]
Alginate	flow-focusing microfluidics	Merging of alginate-cell and $CaCl_2$ droplets		Decrease in final concentration of alginate in the droplets	HCT116 cells[38]
Alginate	flow-focusing microfluidics	Incorporation of $CaCO_3$ particles in alginatecell droplets and calcium release upon diffusion of acetic acid from the oil phase into the droplets	Internal gelation without a decrease in final alginate concentration in the droplets	Potential cytotoxicity of $CaCO_3$ particles	9E10 cells murine M6C cells[54]
Alginate	flow-focusing microfluidics	Diffusion of $CaCl_2$ from the oil phase into the droplets through an additional junction	Gelation without a decrease in the final concentration of alginate in the droplets	inhomogeneous hydrogelation due to heterogenous distribution of calcium ions in the droplet	MCF–7, HepG2, and U937 cells [55]
RGD-conjugated alginate with fibrinogen	flow-focusing microfluidics	Release of calcium ions from the soluble CaEDTA complex upon diffusion of acetic acid from the oil phase into the droplets	Internal gelation without potential cytotoxicity of particles	Low single cell encapsulation efficiency	hMSCs[51]
RGD-conjugated alginate, alginate/ collagen	flow-focusing microfluidics	Pre-coating cells with $CaCO_3$ particles	Gelation of only cell-laden droplets leading to high yields	Potential cytotoxicity of $CaCO_3$ particles	mMSCs OP9 pre-adipocyte cells[56]
PEGDA	flow-focusing microfluidics coupled with FACS	UV crosslinking via photoinitiators in both aqueous and oil phases	High single cell encapsulation efficiency and low cell escape from the microgels	Costly and time consuming	hMSCs chondrocytes[39]

Acta Biomater. Author manuscript; available in PMC 2020 September 01.

Materials used	Strategy	Solidification/Crosslinking method	Advantages	Disadvantages	Cell types encapsulated
Star-shaped PEG with RGD moieties	flow-focusing microfluidics	Pre-coating cells with $CaCO_3$ particles & covalent crosslinking catalyzed by calciumactivated FXIII enzyme	Gelation of only cell-laden droplets leading to high yields	Potential cytotoxicity of $CaCO_3$ particles and reduced enzymatic activity upon reduction in pH for calcium release	hMSCs[57]
Dex-TRA or DexTRA/HA-TRA	flow-focusing microfluidics	Delayed crosslinking by HRP via controlled diffusion of H_2O_2 through PDMS walls into the droplets	Positioning of cells in the center of the microgels resulting in low cell escape	Potential cytotoxicity of H_2O_2	hMSCs[58]

Table 2.

Strategies for the nanoencapsulation of single mammalian cells.

Approach	Materials used	Strategy	Advantages	Disadvantages	Cell types encapsulated
Electrostatic deposition	PLL/HA, PLL/ fullorene-PEI, PLL/ RGD, GL/AL, GL/HA, CH/AL, PLL/AL,PAH-SPIONs, PDADMAC/ PSS, ɛPLL/PSS, PAH/PAA	Deposition of polyelectrolytes by centrifugation-based LbL coating	Many synthetic and natural polyelectrolytes can be deposited unselectively on any type of mammalian cells	Polycations may disrupt membrane integrity and centrifugation steps may impair cell viability	mMSCs [70], Jurkat cells [71], hMSCs [72], rabbit platelets [76] hNSCs [77], rat PC12 cells [4], mouse T cells [5]
Electrostatic deposition	CH-PC/AL + PLL-PEG/AL	Deposition of polyelectrolytes by LbL coating using filtration membrane	Filtration membrane shortens the process of LbL coating and significantly improves cell viability	It is hard to balance the concentration of cells and polyelectrolytes to obtain full cell coverage without aggregation	hRBCs[79]
Electrostatic deposition	GL-A/GL-B (inner layer) & PEG (outer layer)	Deposition of polyelectrolytes by centrifugation-based LbL coating followed by thiol-ene crosslinking of PEG	The succinimide thioether group allows for on-demand degradation of PEG layer through reduction by GSH	Poor charge density of gelatin type A requires chemical modification to form a firm inner layer	HeLa cells [11]
Biomineralization	CH/PAA/$LnPO_4$, PEI/SiO_2, $(RKK)_4D_8$/TiO_2	Deposition of polyelectrolytes followed by minerals by LbL-centrifugation coating	A tough layer of mineral is formed on the cells, providing structural support and resistance	Non-degradability of the tough barrier may impair long-term attachment or proliferation of the cells	Zebrafish egg [84], HeLa, NIH3T3 [85], and Jurkat cells [85, 86]
Receptor-ligand interactions	FN/GL, Col-IV/LN, ColI/HA, Col-I triple helix, Nap-FFG	Recognition and binding of cell adhesive sequences to surface receptors such as integrins and CD44	Nanolayers with no net positive charge preserve cell viability, cell adhesive sequences provide additional survival signals to the cells	Relatively fast biodegradation of ECM-based macromolecules is not suitable for long-term cell encapsulation	HepG2 cells [9, 89], iPSC-CMs, rat CMs [90], rMSCs [3], human dermal fibroblasts [91], human platelets [92]
Non-specific interactions	TA-Fe(III)	Deposition of TA on cell surface followed by formation of metal-organic complex by incorporation of Fe(III)	The strategy can be applied to any material with catechol groups for coordination-driven assembly, complexation with Fe(III) allows for controlled degradation using EDTA	Cytotoxicity of Fe(III) irons obliges careful optimization of its concentration to balance crosslinking density and cell viability	HeLa cells, NIH3T3 fibroblasts, Jurkat T cells [93], hRBCs [94]
Non-specific interactions	PG	Deposition of PG on cell surface and oligomerization by autooxidation	Deposition at mild alkaline conditions leads to high cell viability	High hydrophilicity of nanocoating was found to impair oxygen diffusion rate	HeLa cells, hRBCs[95]
Membrane modification	Polyacrylate	*In situ* polymerization on the acrotylated membrane proteins	Surface modification and in situ polymerization under mild conditions preserves cell viability	Mechanically and chemically stable nanolayers were found to impair cell attachment and proliferation	HeLa cells, hMSCs,BACs[97]
Cell surface modification	Maleimide-conjugated CS or PEG	Click chemistry reaction between the thiol groups of reduced membrane proteins and maleimide groups of polymer chains	Coated cells can be covalently incorporated into macrogels without harsh crosslinking conditions	Concentration of the reduction agent TCEP needs to be optimized carefully to preserve cell viability	HeLa cells [98]

Acta Biomater. Author manuscript; available in PMC 2020 September 01.

Approach	Materials used	Strategy	Advantages	Disadvantages	Cell types encapsulated
Cell surface modification	Ph-HA, Ph-AL, Ph-GL, PhPVA	In situ hydrolyzation catalyzed by HRP immobilized on cell surface via conjugation to BAM inserted into plasma membrane or to anti-surface antigen antibodies	Any material conjugated with hydroxy phenyl groups can be used for nanoencapsulation, antibodyconjugated HRP provides cellselectivity	BAM groups induce production and secretion of reactive oxygen species by the cells, H_2O_2 may impair cell viability	STO, HeLa, human epithelial [99] and HepG2 [99, 101] cells

Table 3.

Protection of encapsulated single animal cells against environmental stresses.

Approach	Shell type	Cell type	Protection against	Reference
Microencapsulation	Agarose-(f/f)	hMSC	Anoikis In vivo clearance	[1]
	Agarose-(f/f)	hCSC	Anoikis In vivo clearance	[2]
	PEGDA	hMSC	Antibody	[39]
	Alginate	mMSCs, OP9	Physical force In vivo clearance	[56]
Nanoencapsulation	$LnPO_4$	Zebrafish egg	UV irradiation	[84]
	(CH/AL)/(PLLPEG/AL)	hRBC	Antibodies	[79]
	FN/GL, Col-IV/LN	HepG2	Physical force	[9]
	SiO_2	HeLa	Polycations Proteolytic enzymes	[85]
	TA-Fe(III)	HeLa, NIH3T3, Jurkat	UV irradiation Polycations	[93]
	Polyacrylamide	HeLa	Polycations Antibodies	[97]
	PG	hRBC	Antibodies	[95]
	CH/AL	Murine T	GVHD	[5]
	(GL-A/GL-B)-PEG	HeLa	Polycations Proteolytic enzymes Antibodies Physical forces	[11]
	Col/HA	hMSC	Anoikis	[3]
	(PLL/RGD)/(PLL/HA)	hMSC	Physical force	[72]
	TA-Fe(III)	hRBC	Antibodies	[94]
	TiO_2	Jurkat	Non-culture temperature	[10]
	GL/HA	rat PC12	Apoptotic cytokines	[4]
	PEG & MSNs	HeLa	In vivo clearance	[98]